Remote Sensing of Environment 266 (2021) 112716

Contents lists available at ScienceDirect

Remote Sensing of Environment

journal homepage: www.elsevier.com/locate/rse

Multiscale assessment of land surface phenology from harmonized Landsat 8 and Sentinel-2, PlanetScope, and PhenoCam imagery

Minkyu Moon [a,*], Andrew D. Richardson [b,c], Mark A. Friedl [a]

[a] Department of Earth and Environment, Boston University, Boston, MA 02215, USA
[b] School of Informatics, Computing, and Cyber Systems, Northern Arizona University
[c] Center for Ecosystem Science and Society, Northern Arizona University

ARTICLE INFO

Editor: Dr. Marie Weiss

Keywords:
Land surface phenology
Vegetation indices
Landsat
EVI2
Sentinel-2
PlanetScope
PhenoCam

ABSTRACT

As the spatial and temporal resolution of remotely sensed imagery has improved over the last four decades, algorithms for monitoring and mapping seasonal changes in surface properties have evolved rapidly. Most recently, the availability of daily PlanetScope imagery has created new opportunities for monitoring the land surface phenology (LSP) of terrestrial ecosystems at high spatial resolution. However, the quality and value of LSP information from PlanetScope imagery have not been systematically examined. In this paper, we evaluate the character and quality of LSP information derived from PlanetScope by comparing time series of vegetation indices and LSP metrics from PlanetScope to corresponding time series and LSP metrics derived from Harmonized Landsat 8 and Sentinel-2 (HLS) imagery and PhenoCams at six sites that span a diverse range of land cover types and climate. Results show that vegetation index time series from all three data sources show high temporal correlation, and LSP metrics derived from HLS, PlanetScope, and PhenoCam show high agreement with negligible bias. Semi-variograms for phenometrics estimated from PlanetScope imagery indicate that the majority of spatial variance captured in PlanetScope phenometrics occurs well below the spatial resolution HLS imagery. At the same time, LSP metrics from HLS are most strongly correlated with the 50–75% quantiles of 3 m LSP metrics from PlanetScope. This indicates that HLS captures the average phenology at sub-pixel scale captured in PlanetScope imagery. Our results represent the first comprehensive comparison of LSP metrics estimated from PlanetScope and publicly available moderate spatial resolution imagery, and provide insights regarding: (1) the quality and character of LSP metrics derived from HLS and PlanetScope; and (2) the relative merits and trade-offs associated with the use of each data source for LSP studies.

1. Introduction

Time series of optical remote sensing imagery have been used to measure land surface phenology (LSP) for nearly four decades (Justice et al., 1985) and are widely used to characterize seasonal-to-decadal scale dynamics and changes in ecosystem properties and function (Berra and Gaulton, 2021; Morisette et al., 2009; Piao et al., 2019; Zeng et al., 2020). In ecosystems dominated by natural vegetation, LSP measurements have been used to measure the impact of climate change on the timing and duration of growing seasons (Liu et al., 2018; Park et al., 2016), to assess the feedbacks of vegetation phenology on land-atmosphere interactions (Moon et al., 2020; Richardson et al., 2013; Young et al., 2021), and to quantify the sensitivity of ecosystem phenology to climate change (Friedl et al., 2014; Moon et al., 2021; Seyednasrollah et al., 2020b). In croplands, LSP measurements are useful for distinguishing crop types, identifying management practices such as double cropping, and modeling crop yields (Cai et al., 2018; Chaves et al., 2020; Diao, 2020). More generally, remotely sensed features based on LSP metrics are widely exploited for mapping land cover and land-use changes (Nguyen et al., 2020; Sulla-Menashe et al., 2019; Zhu and Woodcock, 2014).

Early LSP research leveraged bi-monthly composites of vegetation indices from AVHRR (Jonsson and Eklundh, 2002; Justice et al., 1985; Reed et al., 1994), and subsequently, 8-day composites from MODIS (Ganguly et al., 2010; Jönsson et al., 2010; Zhang et al., 2003). These studies demonstrated the power of LSP measurements for monitoring ecosystem dynamics over large areas. However, the coarse spatial resolution of AVHRR and MODIS limits their utility for applications that

* Corresponding author at: 685 Commonwealth Avenue, Boston, MA, 02215, USA.
E-mail address: moon.minkyu@gmail.com (M. Moon).

https://doi.org/10.1016/j.rse.2021.112716
Received 8 December 2020; Received in revised form 17 August 2021; Accepted 23 September 2021
Available online 29 September 2021

require fine-scale information related to phenology. To address this, Fisher and Mustard (2007), Elmore et al. (2012), and Melaas et al. (2016, 2013) (among others) developed methods based on Landsat imagery to estimate LSP at 30 m spatial resolution. Building on these efforts, Bolton et al. (2020) used Harmonized Landsat 8 and Sentinel-2 (HLS; Claverie et al. (2018)) data to create a LSP data set for North America at 30 m spatial resolution.

In the last several years commercial PlanetScope imagery has become available, providing new opportunities for LSP measurements at high spatial resolution. PlanetScope imagery is acquired by a constellation of CubeSats (180+ as of 2021; Planet, 2021), and provides daily imagery for the entire Earth in four bands spanning the visible and near-infrared wavelengths at 3 m spatial resolution. Although PlanetScope data do not have the scientific quality of publicly available moderate spatial resolution imagery such as Landsat 8 and Sentinel-2 (Dash and Ogutu, 2016; Houborg and McCabe, 2018; Wang et al., 2020), the spatial and temporal resolution of PlanetScope imagery creates new opportunities to investigate a wide array of land surface properties and processes including near real-time monitoring of carbon emissions (Csillik and Asner, 2020), land cover and land-use changes (Qayyum et al., 2020), crop monitoring (Breunig et al., 2020; Kimm et al., 2020), species mapping (Wicaksono and Lazuardi, 2018), and vegetation phenology (Cheng et al., 2020; Dixon et al., 2021; Wang et al., 2020). To date, however, no study has explored the effectiveness and accuracy of PlanetScope imagery for estimating and monitoring LSP across multiple ecosystem types and climate zones.

In this paper, we explore the quality and utility of high spatial resolution daily imagery from PlanetScope for estimating fine-scale data LSP across a diverse range of vegetation and land cover types. Specifically, this paper has two primary objectives: (1) to evaluate the density and quality of surface reflectance and vegetation index time series from PlanetScope relative to corresponding time series from NASA's HLS product and vegetation index time series measurements acquired using ground-based PhenoCams; and (2) to compare and assess agreement in LSP metrics estimated from PhenoCams, PlanetScope, and HLS. To address these objectives, we used multiple years of PlanetScope, HLS, and PhenoCam imagery acquired at six sites that span a wide range of climate and land cover types.

2. Methods

2.1. Data and study sites

The HLS data set includes harmonized time series of Landsat 8 and Sentinel-2A and -2B surface reflectance imagery at 30 m spatial resolution with a nominal repeat frequency of ~4 days at the equator and more frequent observations poleward. For this work, we used Version 1.4 of HLS. A detailed technical description of this data product is presented in Claverie et al. (2018). PlanetScope provides daily imagery in the red, green, blue, and near-infrared wavelengths. The ground sample distance between PlanetScope pixels varies as a function of satellite altitude, but averages 3.7 m. The 'Analytic Ortho Scene' product, which we use here, is resampled to a uniform spatial resolution of 3 m (Planet, 2021). These data do not have the radiometric fidelity of HLS imagery (Dash and Ogutu, 2016; Houborg and McCabe, 2018; Wang et al., 2020), but provide daily observations at order-of-magnitude higher spatial resolution relative to HLS. For a more complete description of PlanetScope imagery, the reader is referred to the technical product documentation (Planet, 2021). In this context, it's important to note that while most LSP algorithms are designed to be robust to noise, issues related to undetected clouds, snow, and even uncorrected BRDF effects can compromise the quality of LSP results.

All available HLS and PlanetScope surface reflectance values located within 3 by 3 km windows centered over six study sites equipped with PhenoCams (Table A1 and Fig. A1) for the period 2017–2019 were used in our analysis. For HLS, we screened time series for contamination by clouds and snow at the pixel level (see Bolton et al., 2020). For PlanetScope, we excluded images with more than 10% cloud cover based on metadata included with the imagery, and then excluded all pixel-scale values flagged as contaminated by clouds or snow in the Unusable Data Mask provided with the imagery (Planet, 2021).

In addition to the HLS and PlanetScope data sets, we used time series of near-surface camera imagery and vegetation indices available from the PhenoCam Network (Milliman et al., 2019; Seyednasrollah et al., 2019). Specifically, we used data from 6 PhenoCam sites with 9 cameras that span a range of vegetation, climate, and land cover types including deciduous broadleaf, mixed, and evergreen needleleaf forests, croplands, semi-arid grasslands, and shrublands (DB, MF, EN, AG, GR, and SH, respectively; Table A1 and Fig. A1). With the exception of the cropland site, which has four cameras in adjacent fields with different crops but only one year (2019) of PhenoCam data, we used three years of data for our analysis (2017 to 2019). We included data from 2017 forward because Sentinel-2B was launched in March of 2017, providing the maximum possible temporal sampling in the HLS dataset.

2.2. Assessment of data density

Observation density, and more specifically the number of snow-free and cloud-free images during growing season, is a key factor that controls the quality of LSP retrievals from remotely sensed time series (Zhang et al., 2018b). Therefore, in the first element of our analysis, we quantified the number and timing of clear-sky PlanetScope and HLS observations for individual PlanetScope and HLS pixels at each of the study sites. To do this, we calculated summary statistics (the mean, median, and maximum gap between clear-sky acquisitions) for 1000 randomly selected pixels from each sensor at each site.

2.3. Comparison of vegetation index time series from HLS, PlanetScope, and PhenoCam

In the second element of our analysis, we assessed the agreement among time series of vegetation indices from HLS, PlanetScope, and PhenoCam imagery at each study site. For HLS and PlanetScope, we extracted values for the two-band enhanced vegetation index (EVI2; Jiang et al., 2008) for one HLS pixel and the median of nine co-located PlanetScope pixels (i.e., covering 900 m^2 and 81 m^2 areas for HLS and PlanetScope, respectively) centered over regions of interest (ROI) delineated in PhenoCam imagery (see Fig. 2). For the PhenoCams, we used the green chromatic coordinate (G_{CC}), which has been shown to provide robust time series of canopy greenness (Richardson et al., 2018a; Sonnentag et al., 2012) and has been previously used to assess the quality of LSP metrics from satellite remote sensing (Bolton et al., 2020; Klosterman et al., 2014; Moon et al., 2019; Zhang et al., 2018a).

To assess the agreement between EVI2 time series from HLS and PlanetScope, we computed summary statistics (correlation coefficient (r), root mean square error (RMSE), and bias (PlanetScope - HLS)) at each site. To do this, we used a random sample of 100,000 HLS pixels at each site for dates when both HLS and PlanetScope imagery were available across all three years (i.e., $n = 100{,}000$ pixel-days). As part of this analysis, and to help attribute observed differences between HLS and PlanetScope EVI2 time series, we conducted the same comparison for the near-infrared and red bands in each source of imagery. Note that both analyses compare 30 m HLS values against 3 m PlanetScope values, where each 3 m PlanetScope pixel was randomly selected within each 30 m HLS pixel. Further, to explore how differences in the spatial resolution of HLS and PlanetScope imagery affect our results, we extracted and sorted EVI2 values for all 100 PlanetScope pixels located within each of the 100,000 randomly sampled HLS pixel-days. We then used these data to measure the agreement (correlation, RMSE, and bias) between EVI2 derived from HLS and each quantile of PlanetScope EVI2 values located within HLS pixels.

2.4. Assessment of phenological metrics

To estimate phenological metrics (hereafter phenometrics), we used the algorithm described by Bolton et al. (2020), which extracts the timing of key phenological transition dates during the growing season. For HLS, we used the Multi-Source Land Surface Phenology Yearly North America 30 m Version 1 product (MSLSP30NA) (Friedl, 2020). For PlanetScope, we adapted the algorithm described by Bolton et al. (2020) to exclude HLS-based snow and cloud-screening sub-routines (which are not directly transferable to PlanetScope imagery) and replaced outliers and dormant season values (i.e., values from January, February, November, and December) with PlanetScope EVI2 values corresponding to the 90th percentile of dormant season values. We adopted this approach because screening for snow is challenging in PlanetScope imagery and because the higher frequency of observations provided by PlanetScope leads to fewer gaps. As we show below, this approach yielded highly comparable time series of EVI2 from HLS and PlanetScope.

Using time series of EVI2 from both HLS and PlanetScope, we retrieved the timing of greenup onset, mid-greenup, maturity, peak EVI2, greendown onset, mid-greendown, and dormancy at each pixel, which correspond to the day of year (DOY) when the EVI2 time series exceeds 15%, 50%, 90% of EVI2 amplitude during the greenup phase, reaches its maximum, and goes below 90%, 50%, 15% of EVI2 amplitude during the greendown phase, respectively (Bolton et al., 2020). In addition, we extract the EVI2 amplitude during the growing season for each HLS and PlanetScope pixel. We then computed summary statistics (correlation, RMSE, and bias) and assessed the agreement between phenometrics derived from HLS and PlanetScope.

In addition to assessing overall agreement, we also explored scaling effects in phenometrics estimated from PlanetScope versus HLS using two approaches. First, similar to our analysis of scaling effects in EVI2 data, we measured agreement between each quantile of each phenometric from PlanetScope at 3 m spatial resolution and corresponding phenometrics derived from 30 m HLS pixels. To do this, we used 3 m PlanetScope data from 100,000 randomly selected HLS pixels across all 7 DOY phenometrics at each of the six study sites in 2019. Second, we computed semi-variograms (Matheron, 1963) for each phenometric at 3 m spatial resolution derived from PlanetScope imagery using 100,000 randomly selected PlanetScope pixels for each site in 2019. We used the resulting semi-variograms to assess the magnitude and length scale of spatial variability captured in PlanetScope imagery.

Lastly, to provide a ground-based and independent basis for assessing the realism and quality of phenometrics from HLS and PlanetScope, we compared mid-greenup and mid-greendown dates (i.e., corresponding to the 50% amplitude crossing dates) from each source of imagery against corresponding values estimated from PhenoCam G_{CC} time series. To do this, we compared the 50% greenup and 50% greendown dates provided in the PhenoCam v2.0 data product (Milliman et al., 2019) with corresponding phenometrics estimated from HLS and PlanetScope (i.e., mid-greenup and mid-greendown, respectively). Note that to perform this comparison we used phenometrics estimated for individual HLS (30 m) and PlanetScope (3 m) pixels centered over each of the PhenoCam sites.

3. Results

3.1. Data density

PlanetScope and HLS both had larger gaps during wintertime, and the grassland and shrubland sites located in the Western United States had fewer gaps and relatively uniform density of clear-sky acquisitions throughout the year compared to sites in the Eastern regions (i.e., GR and SH versus DB, MF, and EN, respectively; Fig. 1). Overall, the median duration of gaps between clear-sky and snow-free HLS acquisitions during the growing season, defined here as March 1 through October 31, ranged from 4.1 to 11.0 days across all sites and years (Table 1). As expected, PlanetScope imagery had higher frequency of clear-sky acquisitions, with median duration of gaps between clear-sky and snow-free acquisitions ranging from 1.0 to 3.9 days across all sites and years. For completeness, we provide results that include all available imagery (i.e., including November through February) as an appendix (Table A2).

3.2. Cross-sensor comparison of vegetation index time series

Figs. 2, 3, and 4 show time series from 2017 to 2019 of EVI2 from HLS and PlanetScope and G_{CC} from PhenoCam, along with true-color PlanetScope and PhenoCam images for each site. Time series for each vegetation index across all six sites (Figs. 2d–e, 3f–i, and 4e–h) illustrate the density of observations provided by each source of imagery, as well as the overall agreement in phenology across the three sensors. The deciduous forest and cropland sites (Figs. 2d, 3f–i, and 4e), each of which experience strong seasonal variation in leaf area, show the largest dynamic range in vegetation indices. Conversely, seasonal variation in EVI2 and G_{CC} are lowest at the grassland and shrubland sites (Fig. 4g and h). At the croplands site, differences in phenology associated with different crop types are clearly identifiable in time series captured by each sensor (Fig. 3b–e).

Surprisingly, EVI2 and G_{CC} time series acquired over evergreen

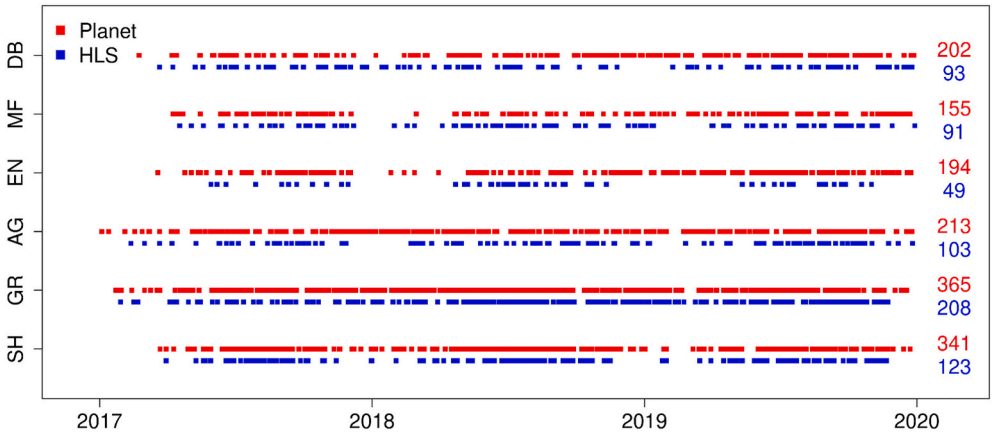

Fig. 1. Clear-sky acquisitions for HLS and PlanetScope pixels centered over the PhenoCam camera location at each site for 2017–2019. The numbers on the right-hand side indicate the total number of clear-sky views for each data source at each site across all three years. DB: deciduous broadleaf forests; MF: mixed forests; EN: evergreen needleleaf forests; AG: croplands; GR: grasslands; SH: shrublands. Table A1 provides site-specific information for each PhenoCam site.

Table 1
Duration of data gaps (in days) between clear-sky acquisitions of HLS and PlanetScope imagery from March to October estimated from 1000 randomly selected pixels located in a 9 km^2 area centered over the PhenoCam at each site.

		2017		2018		2019		All	
		Planet	HLS	Planet	HLS	Planet	HLS	Planet	HLS
DB	Mean	6.2	12.3	5.0	9.4	3.6	9.5	4.9	10.4
	Median	3.1	10.2	4.0	5.6	2.6	7.5	3.2	7.8
	Maximum	31	30	29	32	18	35	31	35
MF	Mean	5.5	11.5	7.9	7.7	4.9	8.8	6.1	9.3
	Median	4.0	10.1	4.6	5.4	3.0	6.9	3.9	7.5
	Maximum	27	23	52	25	23	25	52	25
EN	Mean	5.6	18.1	6.5	10.7	3.6	11.9	5.3	13.6
	Median	3.0	13.6	4.0	8.8	3.0	10.7	3.3	11.0
	Maximum	35	39	40	30	13	31	40	39
AG	Mean	4.6	11.2	2.7	7.7	3.1	7.7	3.5	8.8
	Median	2.6	9.2	1.0	5.4	2.0	5.2	1.9	6.6
	Maximum	20	30	19	25	14	35	20	35
GR	Mean	3.5	6.9	2.3	3.7	2.5	4.0	2.8	4.9
	Median	2.0	6.5	2.0	2.8	2.0	3.0	2.0	4.1
	Maximum	20	18	15	23	10	15	20	23
SH	Mean	2.7	6.4	2.2	5.4	2.4	5.9	2.5	5.9
	Median	1.0	5.0	1.0	4.1	1.0	5.0	1.0	4.7
	Maximum	19	23	11	25	22	17	22	25

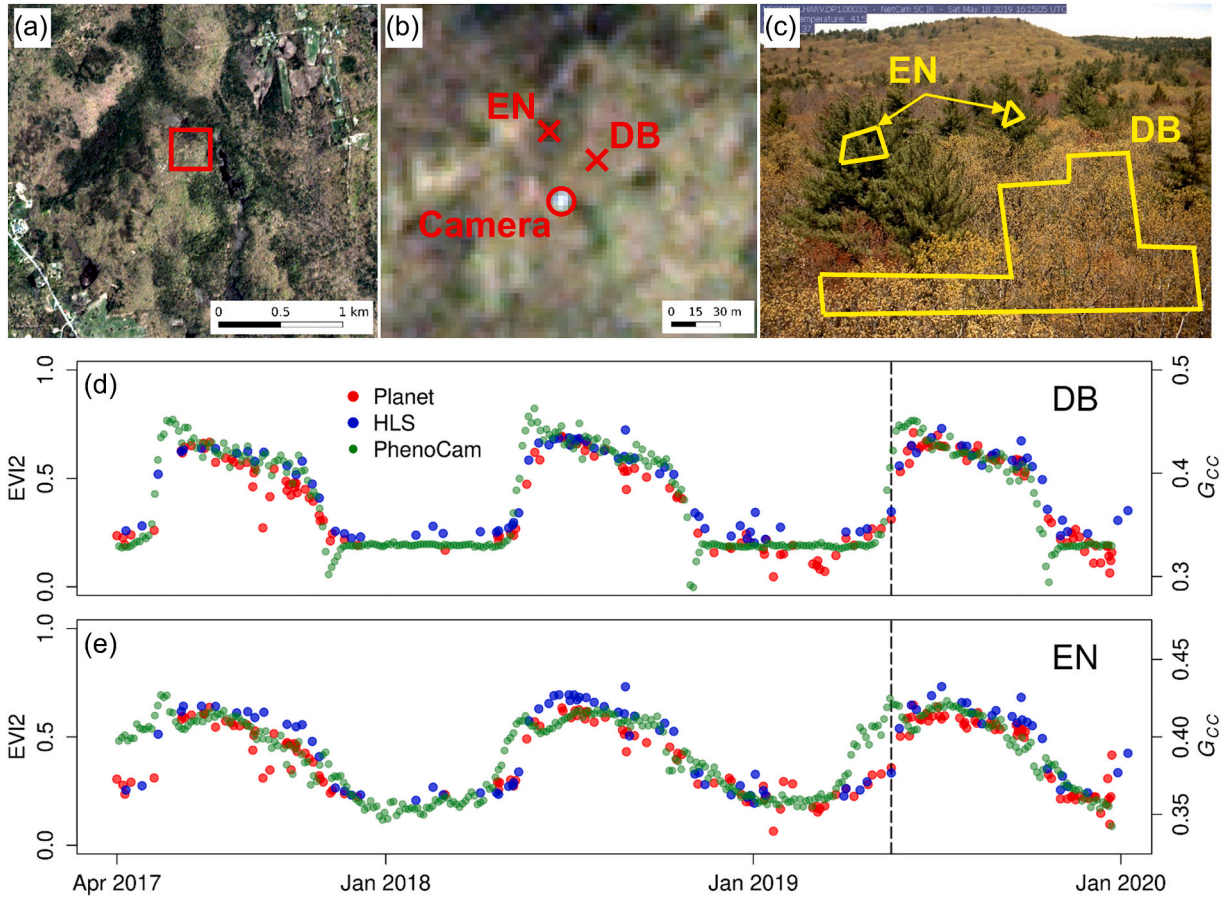

Fig. 2. PlanetScope and PhenoCam images along with time series of vegetation indices from PlanetScope, HLS, and PhenoCam imagery at the mixed forest site. The images in panels (a)-(c) were all acquired on May 18th, 2019, which is identified by the vertical lines in panels (d) and (e). Panel (a) shows a 3 × 3 km PlanetScope image for an area centered over the PhenoCam, which is located inside the red box (panel (b)). Panel (c) shows the regions of interest (ROIs) used to extract G_{CC} time series for deciduous broadleaf (DB) and evergreen needleleaf trees (EN) from PhenoCam images. Panels (d) and (e) show time series of vegetation indices from PlanetScope (red dots) and HLS imagery (blue dots), along with G_{CC} time series (green dots) for the PhenoCam ROIs. (For interpretation of the references to color in this figure legend, the reader is referred to the web version of this article.)

needleleaf forests (Figs. 2e and 4f) show seasonal variation that is nearly as large as the seasonal variation in deciduous forests (Figs. 2d and 3e). The PhenoCam site in Fig. 2 is dominated by mixed forest. Hence, some of the seasonal variation in Fig. 2f may be related to broadleaf species in the overstory or understory that are visible in the sensor fields of view for Landsat 8, Sentinel-2, and the PlanetScope. The forest canopy at the

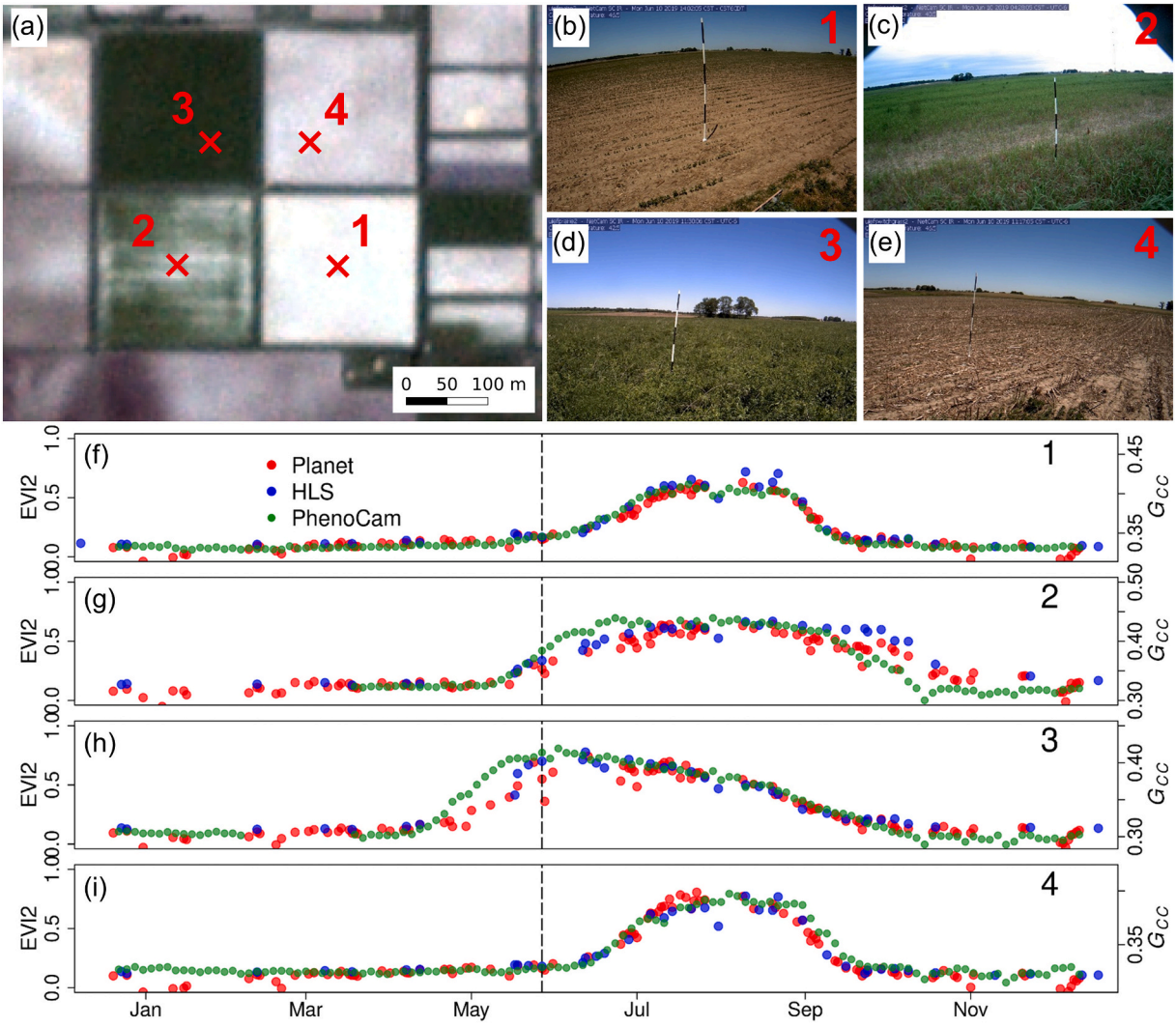

Fig. 3. PlanetScope and PhenoCam images, along with time series of vegetation indices from PlanetScope, HLS, and PhenoCams for the cropland site. The PlanetScope (panel (a)) and PhenoCam images (panels (b)–(e)) were acquired on June 10th, 2019, which is identified by the vertical lines in panels (f)–(i). Panels (f)–(i) show time series of vegetation indices from PlanetScope (red dots) and HLS imagery (blue dots), along with G_{CC} time series (green dots) for the PhenoCam ROIs. The red ×'s in panel (a) shows the PhenoCam camera locations. Numbers in the upper right corner of panels (b)–(e) and (f)–(i) identify the fields from which each time series was extracted. (For interpretation of the references to color in this figure legend, the reader is referred to the web version of this article.)

evergreen needleleaf forest site (Fig. 4b, f), on the other hand, is dominated by conifers, but includes roughly 10% deciduous species; hence, part of the seasonality in EVI2 at this site may be caused by deciduous tree species in the sensor fields of view. Further, Seyednasrollah et al. (2021) demonstrated that seasonality in G_{CC} time series at conifer sites is strongly correlated with changes in pigments, which may also explain some of the seasonality in EVI2.

To illustrate the range of variability and correspondence in phenology detected by each of the sensors across different ecosystems, Fig. 4 shows time series for 2017–2019 across four sites with different plant functional types that span a diverse range of climate regimes (deciduous broadleaf forests, evergreen needleleaf forests, grasslands, and shrublands). Visual inspection of Fig. 4h suggests that HLS EVI2 data may have modestly lower sensitivity to phenology in shrublands relative to PlanetScope EVI2 and PhenoCam G_{CC}. However, the overall agreement in time series, even in ecosystems with relatively weak phenology, was remarkably strong ($r = 0.84$–0.98). It's also worth noting that G_{CC} values from some of the PhenoCams start increasing (and reach their peak) slightly earlier in spring than EVI2 time series from either PlanetScope or HLS (Figs. 2d, e, and 3h), after which G_{CC} closely tracks EVI2 for the rest of the season. This requires more investigation but is likely a by-product of the oblique view-angle used by the PhenoCams and/or differences in the spectral bands used to compute G_{CC} from PhenoCam and EVI2 from HLS and PlanetScope (Keenan et al., 2014).

Overall agreement between 30 m EVI2 from HLS and 3 m EVI2 from PlanetScope was high (Fig. 5). Correlation was lowest at the shrubland site ($r = 0.77$), which reflects the low amplitude of variation in EVI2 at this site. Interestingly, results shown in Fig. 5 indicate that EVI2 values from HLS were systematically higher than those from PlanetScope by ~0.01–0.05, depending on vegetation type. Comparison of red and near-infrared reflectance values from HLS and PlanetScope (Figs. A2 and A3) shows that near-infrared reflectances from HLS and PlanetScope are highly correlated with negligible bias, but that surface reflectances in the red band of PlanetScope were systematically higher than corresponding reflectances from HLS (Figs. A2, A3), which causes HLS EVI2 values to be higher than PlanetScope EVI2 values.

Patterns of agreement in EVI2 from HLS and PlanetScope across quantiles of PlanetScope EVI2 at subpixel scale show strong correspondence across all quantiles (Fig. 6). Consistent with results shown in Fig. 5, correlation between 30 m HLS and 3 m PlanetScope EVI2 quantiles was generally strong (ranging from 0.75–0.97), was lowest in vegetation with weak seasonality (shrublands) and highest in vegetation

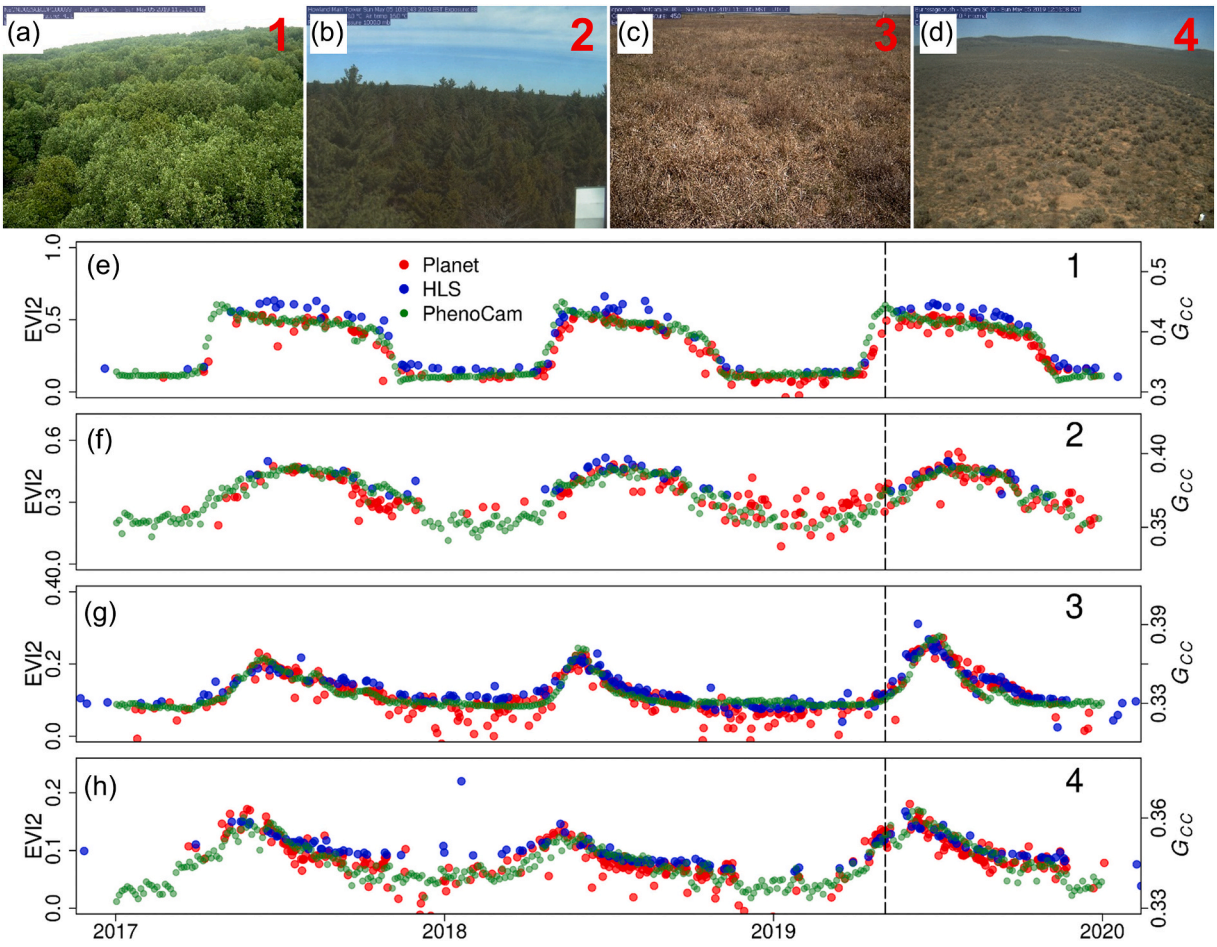

Fig. 4. PhenoCam images along with time series of vegetation indices from PlanetScope, HLS, and PhenoCam imagery for four different vegetation types: (a) deciduous broadleaf forests; (b) evergreen needleleaf forests; (c) grasslands; and (d) shrublands. The PhenoCam images in panels (a)–(d) were acquired on May 5th, 2019, which is identified by the vertical lines in panels (e)–(h). Panels (e)–(h) show time series of vegetation indices from PlanetScope (red dots) and HLS imagery (blue dots), along with G_{CC} time series (green dots) for the PhenoCam ROIs. Numbers in the upper right corner of panels (a)–(d) and (e)–(h) identify the site from which each time series was extracted. (For interpretation of the references to color in this figure legend, the reader is referred to the web version of this article.)

with pronounced seasonality (deciduous broadleaf forests), and showed only modest variation within vegetation types, with maximum correlation generally near the 50th percentile in PlanetScope EVI2 values. RMSE and bias were both low, ranging from 0.02 to 0.10 and from −0.08 to 0.01, respectively, and were minimum for larger values of PlanetScope EVI2 (quantiles >90%), which is consistent with the systematic bias we found between HLS and PlanetScope EVI2 values shown in Fig. 5 (i.e., lower EVI2 values in PlanetScope). Overall, these results imply that despite differences in the spatial resolution, spectral bandpasses, and radiometric fidelity of HLS and PlanetScope imagery, the agreement between vegetation indices derived from each source is high. That said, correlation and RMSE show modest systematic variation across plant functional types, with shrublands and evergreen needleleaf forests (which have weaker seasonality) showing modestly lower overall correlation (and higher RMSEs) relative to other cover types.

3.3. Assessment of phenometrics from HLS, PlanetScope, and PhenoCam

Comparison of phenological maps retrieved from HLS versus PlanetScope demonstrates that PlanetScope imagery resolves fine-scale details that are not captured by HLS imagery. To illustrate, Fig. 7 shows PlanetScope imagery and phenometrics for a 3 × 3 km window centered over the PhenoCam at the mixed forest site. The top row of Fig. 7 (a–c) shows a true color PlanetScope image acquired on May 18th, 2019 (DOY 139; just prior to greenup), along with maps showing the estimated DOY corresponding to the timing of 50% greenup and the EVI2 amplitude at each pixel in 2019 from PlanetScope. The lower row of Fig. 7 (d, e) shows the 50% greenup date from HLS and 30 m land cover from the USGS National Land Cover Database. Overall agreement in the spatial pattern of greenup timing is strong, and the spatial distribution of deciduous and evergreen vegetation is clearly discernible in Fig. 7a and c (cf., Fig. 7e). More importantly, the maps shown in Fig. 7a–c illustrate the granularity of fine-scale information related to phenology, land cover, and plant functional types captured by PlanetScope that is not resolved in 30 m HLS imagery (cf., Fig. 7b, c, d). Similar results are shown in Fig. 8 for the cropland site, which includes a wider range of greenup dates arising from cropping and land management practices relative to the mixed forest site. Specifically, comparison of Fig. 8b and d reveals that while HLS imagery resolves some sub-field variation in phenology at 30 m spatial resolution, the granularity of information provided by PlanetScope, both within and across fields, includes substantial variation at fine spatial scale that is not resolved in HLS imagery.

To provide a comprehensive and quantitative comparison of DOY phenometrics estimated from HLS and PlanetScope across the full range of ecosystems included in our analysis, Fig. 9 presents scatterplots showing the relationship between DOY phenometrics from HLS versus PlanetScope at each site. At seasonal time scale (i.e., across phenometrics), correlation between phenometrics from HLS and PlanetScope was high (r = 0.89–0.98) with only modest differences (bias = −4.5 to 1.5 days). However, RMSEs ranged from 14.6 to 28.7 days, which

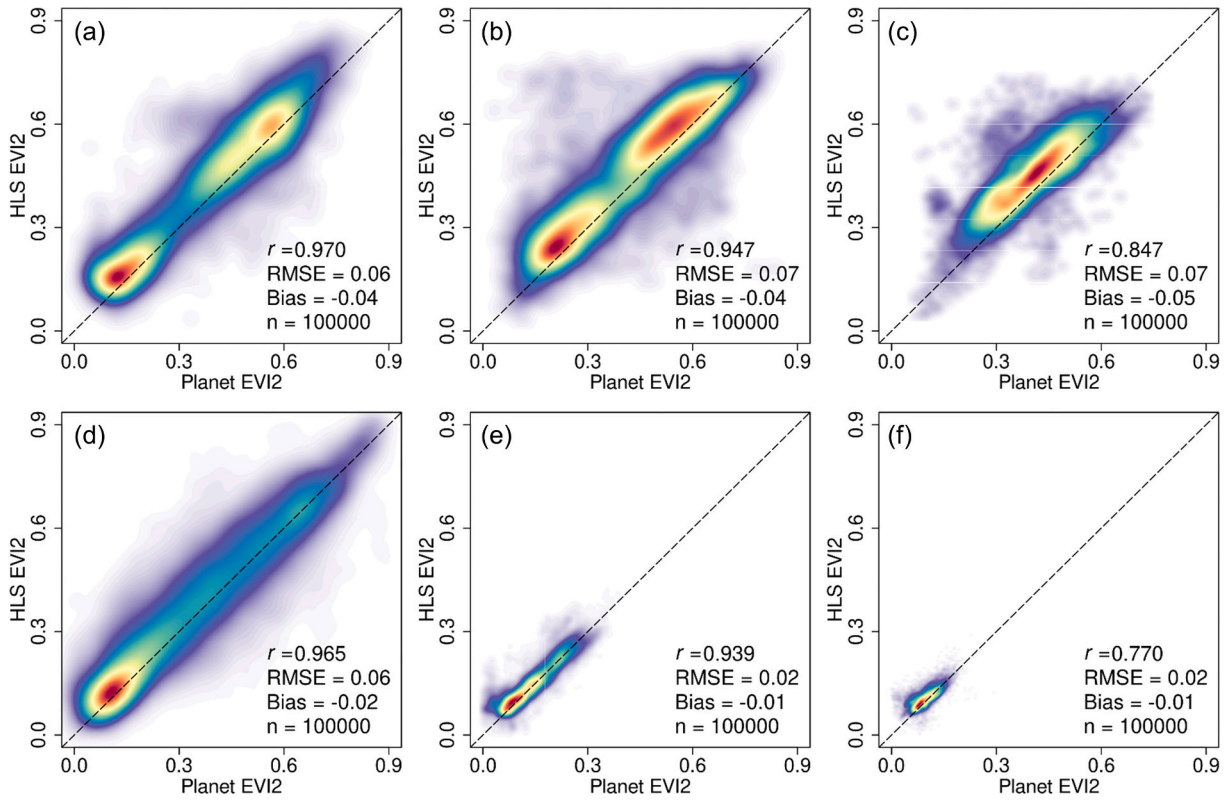

Fig. 5. Comparison of EVI2 from HLS and PlanetScope: (a) deciduous broadleaf forests; (b) evergreen needleleaf forests; (c) mixed forests; (d) croplands; (e) grasslands; and (d) shrublands. PlanetScope EVI2 values were derived from a single randomly selected PlanetScope pixel located within each HLS pixel.

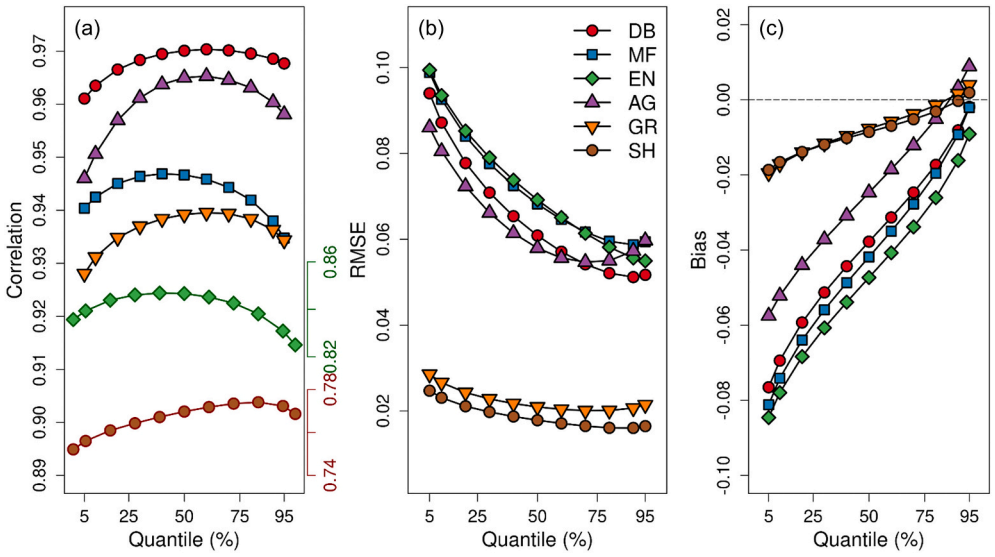

Fig. 6. Empirical relationship between 30 m HLS EVI2 values and PlanetScope EVI2 values at 3 m spatial resolution located within HLS pixels: (a) correlation; (b) root mean squared error (RMSE); and (c) bias (PlanetScope – HLS) between HLS EVI2 values and quantiles in the distribution of PlanetScope EVI2 values located within HLS pixels. Note that EN and SH have different scales from the other land cover types on the vertical axis in panel (a). See the caption for Fig. 1 for definitions of acronyms in the legend.

reflects variability in phenology that occurs below the 30 m resolution of HLS that is captured by PlanetScope imagery. Consistent with this, agreement between individual phenometrics from HLS and PlanetScope at each site was relatively low (Table 2), with average correlations, RMSEs, and biases for each phenometric that ranged from 0.213 to 0.427, from 12.6 to 30.3, and from −9.6 to 4.7, respectively. Across sites, RMSE between HLS and PlanetScope phenometrics was substantially larger at the AG and SH sites, which suggests that spatial variation below 30 m was greater at these sites relative to the DB, MF, EN, and GR sites.

Consistent with results shown in Fig. 9, correlation between quantiles of 3 m phenometrics from PlanetScope and 30 m HLS phenometrics was high ($r > 0.85$), relatively invariant as a function of PlanetScope quantile, and tended to be maximum for the interquartile range (i.e., 25–75%) of PlanetScope phenometric values (Fig. 10a). The one exception was shrublands, where correlation decreased monotonically from 0.95 for the 5th quantile to 0.85 for the 95th quantile (Fig. 10b). Variation in RMSEs mirrored the pattern in Fig. 10a for correlation, and bias (Fig. 10c) tended to be minimum for the 50-75th quantiles across all vegetation types. Together, these results indicate that phenometrics from HLS were broadly representative of average phenology at sub-pixel scale.

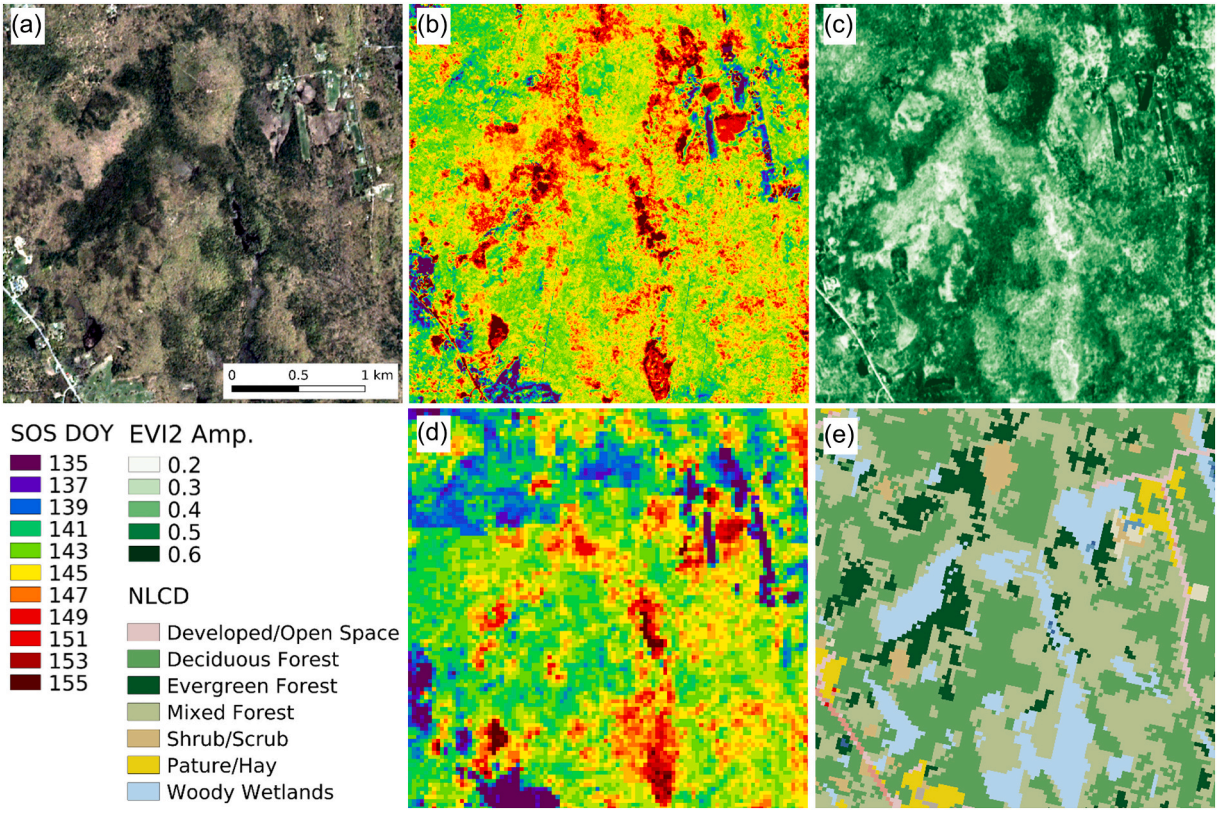

Fig. 7. Phenometrics derived from PlanetScope and HLS at the mixed forest site. Panel (a) shows a true color image from PlanetScope acquired on May 18th, 2019 (DOY 139). Panels (b) and (d) show the DOY corresponding to when EVI2 reaches 50% of its seasonal amplitude during springtime from PlanetScope and HLS, respectively. Panels (c) and (e) show the magnitude of EVI2 seasonal amplitude from PlanetScope and land cover from the USGS National Land Cover Database (NLCD; USGS and Rigge, 2019) in 2016, respectively.

Semi-variograms for LSP metrics derived from PlanetScope imagery at each site demonstrate that spatial variance in 3 m phenometrics consistently asymptote at length scales well below the spatial resolution of HLS, typically at distances of 9–15 m (Fig. 11). With one notable exception, the overall magnitude of spatial variance was relatively uniform (peak semi-variance generally $\leq$25 days) across sites. The timing of 15% and 50% greenup at the DB site was remarkably uniform (i.e., low semi-variance; Fig. 11a); conversely, the 15% greenup and 15% greendown phenometrics at the EN site showed higher semi-variance relative to semi-variances for the other five phenometrics at this site (Fig. 11c). Semi-variance at the AG site was higher than might be expected in managed monoculture fields because phenometrics were sampled across a diverse set of fields with different crop types, management practices, and phenology (Fig. 8). The SH site (Fig. 11f) exhibited the widest range in overall semi-variance, with much higher spatial variance in late-season phenometrics and lower spatial variance in early season phenometrics. This is consistent with the pattern shown in Fig. 9f, where end-of-season phenometrics from PlanetScope exhibited much more variability than corresponding end-of-season phenometrics from HLS, and indicates that the timing of phenology at the end of the growing season is highly variable at short length scales across space at the SH site. It is also worth noting that the nugget variance (and hence the uncertainty in LSP metrics from PlanetScope) in the semi-variograms shown in Fig. 11 are quite variable across phenometrics and sites. The specific mechanisms behind these patterns are unclear and require more investigation.

Finally, comparison of 50% greenup and greendown dates show strong 1-to-1 agreement ($r > 0.97$) with modest bias (<5 days) across all three sources of imagery (Fig. 12). Phenometrics estimated from PhenoCams during springtime at the MF and EF sites were systematically early relative to corresponding phenometrics from HLS and PlanetScope (blue and green circles in Fig. 12a and b). This result is consistent with patterns in Figs. 2, 3, and 4, where G_{CC} values from PhenoCams start to increase and reach their peaks earlier in spring than EVI2 time series from either PlanetScope or HLS. Note that the MF site has two points for each phenometric in each year (12 points total) derived from two different ROIs (one for DB and one for EN) at the site; similarly, the AG site has four points for each phenometric, but data are only available from one year (2019; 8 points total).

4. Discussion

PlanetScope imagery is increasingly being used for scientific applications focused on terrestrial ecosystems. A common use case is land cover and land-use change, where the spatial resolution and temporal frequency of PlanetScope imagery can provide information related to fine-scale land cover changes that may not be captured by moderate spatial resolution sensors such as the Landsat 8 OLI and Sentinel-2 MSI (e.g., Loranty et al., 2018; Pickering et al., 2021). Similarly, the use of PlanetScope imagery to estimate land surface phenology is a natural use case that is becoming more common. For example, John et al. (2020) used PlanetScope imagery to detect the timing of flowering in alpine wildflowers in Washington State, Chen et al. (2019) used PlanetScope imagery in combination with imagery from Sentinel-2 to monitor flowering phenology in almond orchards in the Central Valley of California, and Dixon et al. (2021) used imagery from unmanned aerial vehicles and PlanetScope to model the timing of flowering in Eucalypt trees in Australia. Wu et al. (2021) also used PlanetScope in combination with imagery from unmanned aerial vehicles but focused on autumn phenology in a temperate forest site in Northeastern China. Cheng et al. (2020) compared phenometrics from both PlanetScope and Sentinel-2 (at 10 m) against corresponding phenometrics from PhenoCams and

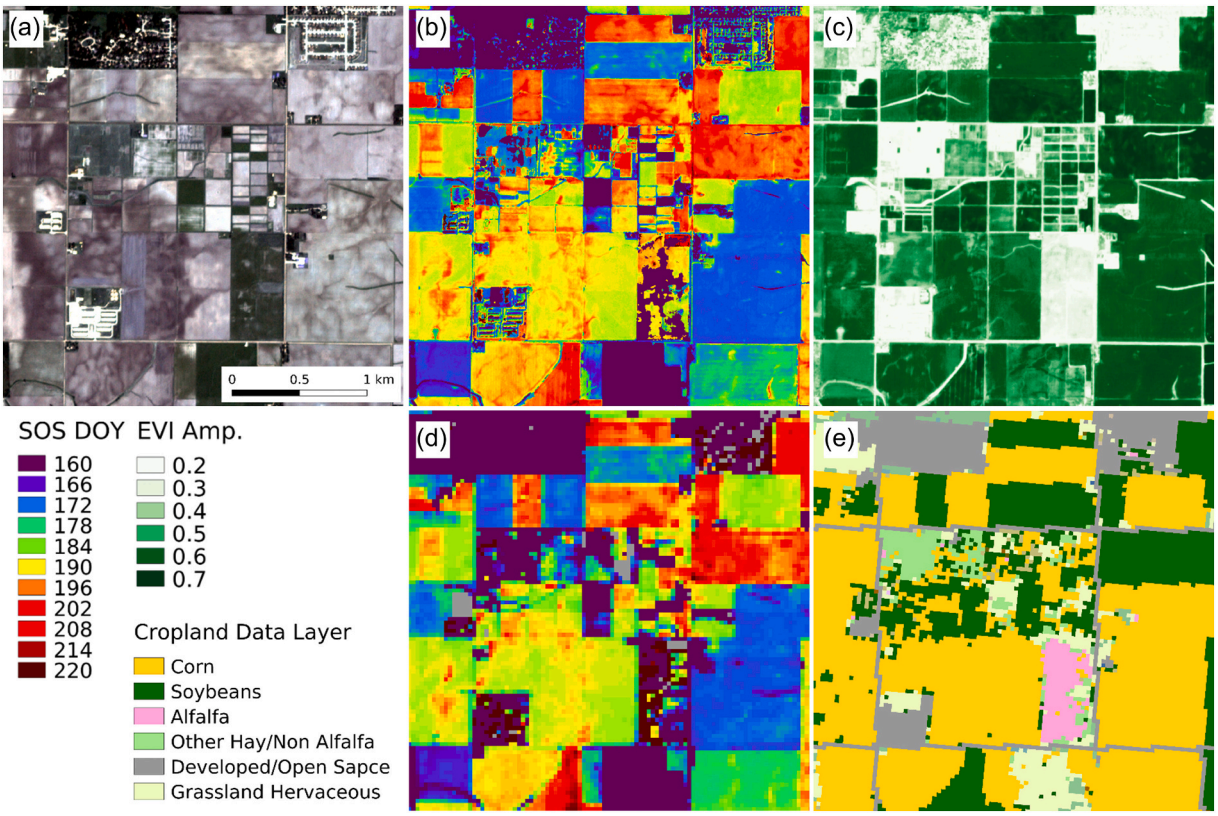

Fig. 8. Phenometrics derived from PlanetScope and HLS for the croplands site. Panel (a) shows a true color image from PlanetScope acquired on June 10th, 2019 (DOY 161). Panels (b) and (d) show the DOY when EVI2 reaches 50% of its seasonal amplitude during springtime from PlanetScope and HLS, respectively. Panels (c) and (e) show the magnitude of seasonal amplitude in EVI2 from PlanetScope and the USDA's Cropland Data Layer (USDA, 2020) in 2019, respectively.

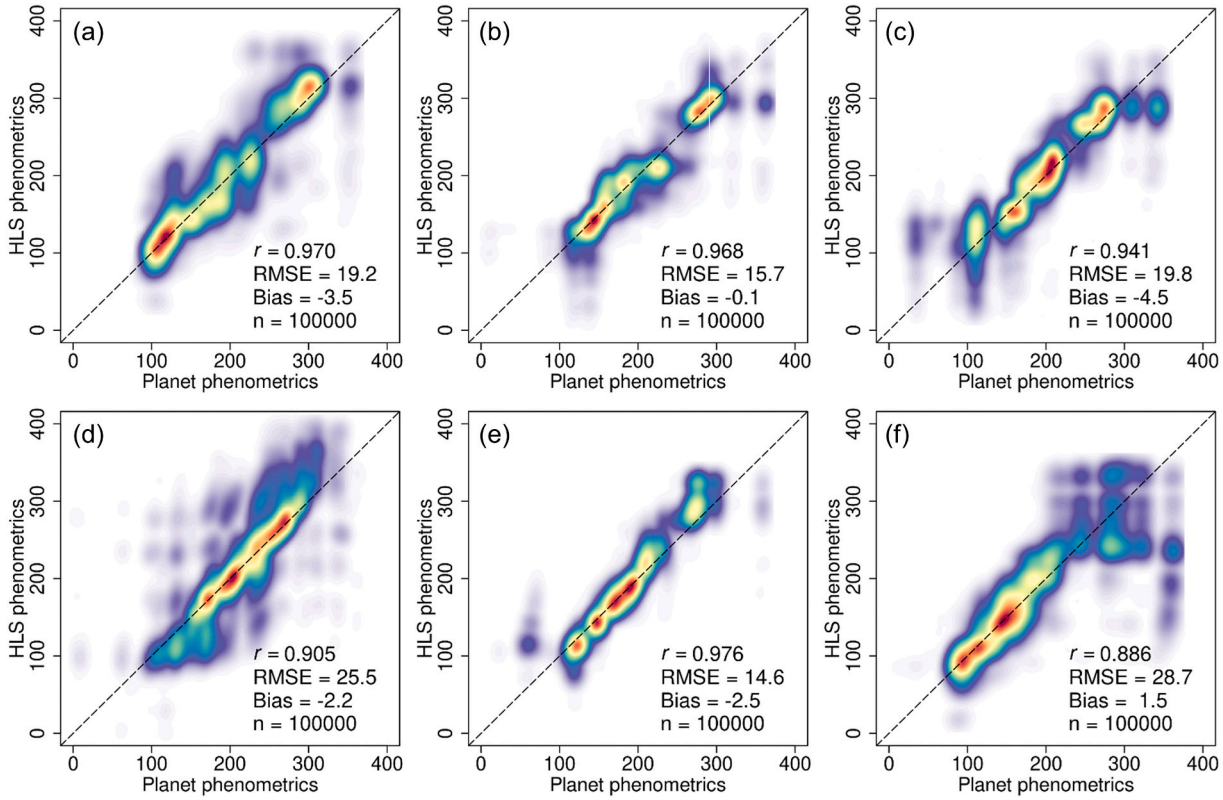

Fig. 9. Scatterplots of DOY phenometrics from HLS versus PlanetScope: (a) deciduous broadleaf forests; (b) evergreen needleleaf forests; (c) mixed forests; (d) croplands; (e) grasslands; and (f) shrublands.

Table 2
Summary statistics comparing DOY phenometrics retrieved from HLS and PlanetScope at each site. Each vegetation type (i.e., each column) represents each PhenoCam site. Table A1 provides site-specific information for each PhenoCam site.

		DB	MF	EN	AG	GR	SH	Average
Greenup onset	*r*	0.294	0.217	0.207	0.620	0.155	0.307	0.300
	RMSE	10.7	16.9	30	27.6	16.3	11.3	18.8
	Bias	4.5	7.8	−6.7	9.5	8.0	5.0	4.7
Mid-greenup	*r*	0.202	0.396	0.082	0.619	0.399	0.448	0.358
	RMSE	8.3	5.5	16.1	24.2	9.2	12.3	12.6
	Bias	−3.3	2.0	4.5	4.7	4.3	5.3	2.9
Maturity	*r*	0.286	0.259	0.226	0.560	0.596	0.261	0.365
	RMSE	16.3	13.5	13.7	23.0	7.9	19.7	15.7
	Bias	−1.4	−3.5	−1.6	2.5	3.0	5.5	0.7
Peak	*r*	0.221	0.110	0.028	0.550	0.599	0.176	0.281
	RMSE	24.1	19.0	13.4	23.2	8.0	21.7	18.2
	Bias	6.0	−6.4	−4.2	−2.0	1.5	−0.6	−1.0
Greendown onset	*r*	0.434	0.206	0.146	0.424	0.687	0.168	0.344
	RMSE	20.3	20.1	16.4	24.0	6.0	24.0	18.5
	Bias	−2.7	8.2	−10.7	−4.2	−1.2	−6.1	−2.8
Mid-greendown	*r*	0.694	0.472	0.242	0.402	0.644	0.107	0.427
	RMSE	20.9	11.4	18.3	23.8	15.8	35.0	20.8
	Bias	−12.5	−5.1	−9.3	−9.6	−12.2	−8.9	−9.6
Dormant	*r*	0.032	0.111	0.097	0.555	0.454	0.029	0.213
	RMSE	26.6	18.7	25.7	30.8	26.9	53.3	30.3
	Bias	−15.3	−3.8	−3.7	−16.4	−21.0	10.7	−8.3

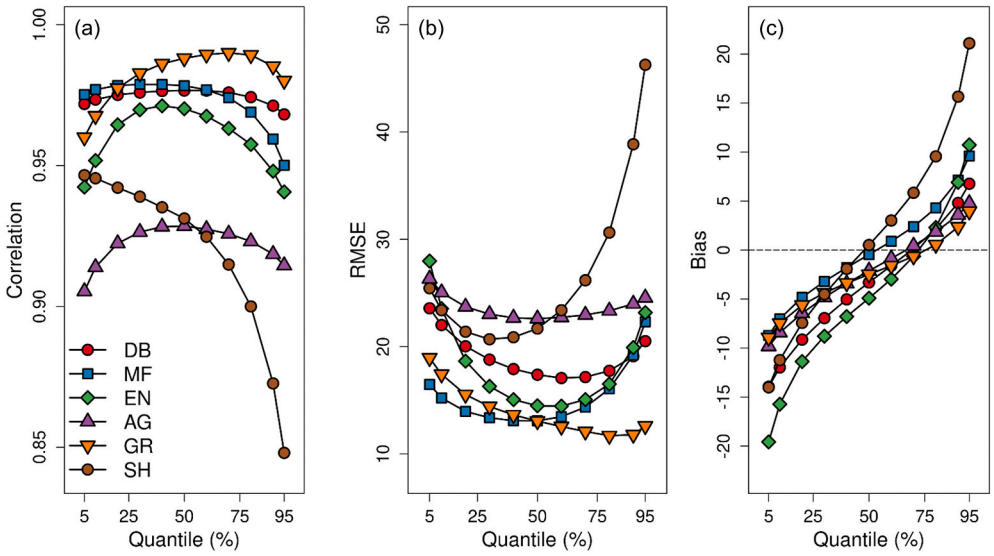

Fig. 10. Empirical relationships between 30 m HLS phenometrics and 3 m PlanetScope phenometrics: (a) correlation; (b) root mean squared error (RMSE); and (c) bias (PlanetScope – HLS) between HLS phenometrics and quantiles in the distribution of PlanetScope phenometric values located within HLS pixels. See the caption for Fig. 1 for definitions of acronyms in the legend.

MODIS at a semi-arid site in Kenya. Using a somewhat different approach, Wang et al. (2020) used PlanetScope in combination with MODIS to monitor dry season phenology in Amazonia. In agriculture, PlanetScope has been used to monitor crop phenology and development (Houborg and McCabe, 2018; Myers et al., 2019; Sadeh et al., 2021).

The studies described above consistently demonstrate that PlanetScope imagery provides an effective basis for monitoring phenology from remote sensing. However, each of the studies discussed above focuses on individual phenological events (or sub-seasons) for a single ecosystem type. To date, no study has systematically assessed the character and quality of vegetation indices and LSP metrics from PlanetScope imagery to corresponding time series and metrics derived at moderate spatial resolution from freely available Landsat 8 and Sentinel-2 imagery. Unlike previous papers, we performed this assessment across multiple growing seasons, ecosystem types, and climate domains. Further, in addition to assessing the correspondence between vegetation indices and LSP metrics from PlanetScope, HLS, and PhenoCams, we explore questions related to scaling and the additional spatial detail in LSP metrics that 3 m PlanetScope imagery provides relative to 30 m HLS imagery.

Our results demonstrate strong overall agreement in phenometrics from HLS, PlanetScope, and PhenoCams across the entire growing season and a wide range of land cover types. We also show that PlanetScope imagery captures substantial fine-scale spatial variation in phenology that is not resolved at moderate spatial resolution by HLS. This result is not a surprise, but is important because it quantifies the nature and character of variation in LSP that is not captured in HLS. Significantly, our results show that LSP metrics from HLS accurately capture the mean phenology at 3 m spatial resolution measured by PlanetScope. This latter conclusion is important because it illustrates how the relative utility of LSP metrics derived from PlanetScope versus HL depends on the application. For use cases that require fine-scale variation in phenology (e.g., high resolution monitoring of crops) our results suggest that PlanetScope imagery provides useful information related to canopy-scale

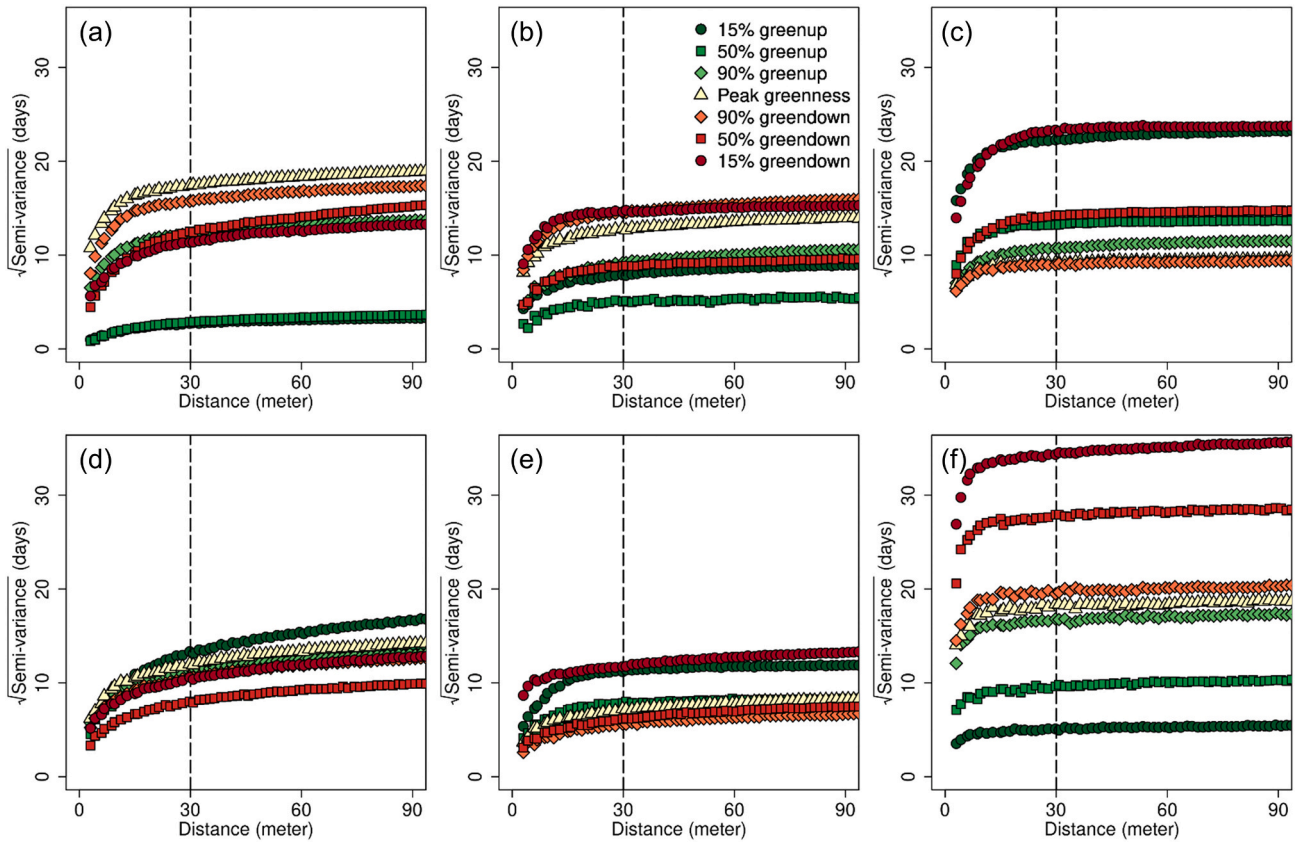

Fig. 11. Semi-variograms from 3 m PlanetScope phenometrics at each site: (a) deciduous broadleaf forest; (b) evergreen needleleaf forest; (c) mixed forest; (d) cropland; (e) grassland; and (f) shrubland. Vertical dashed lines are included to show the spatial resolution of HLS imagery.

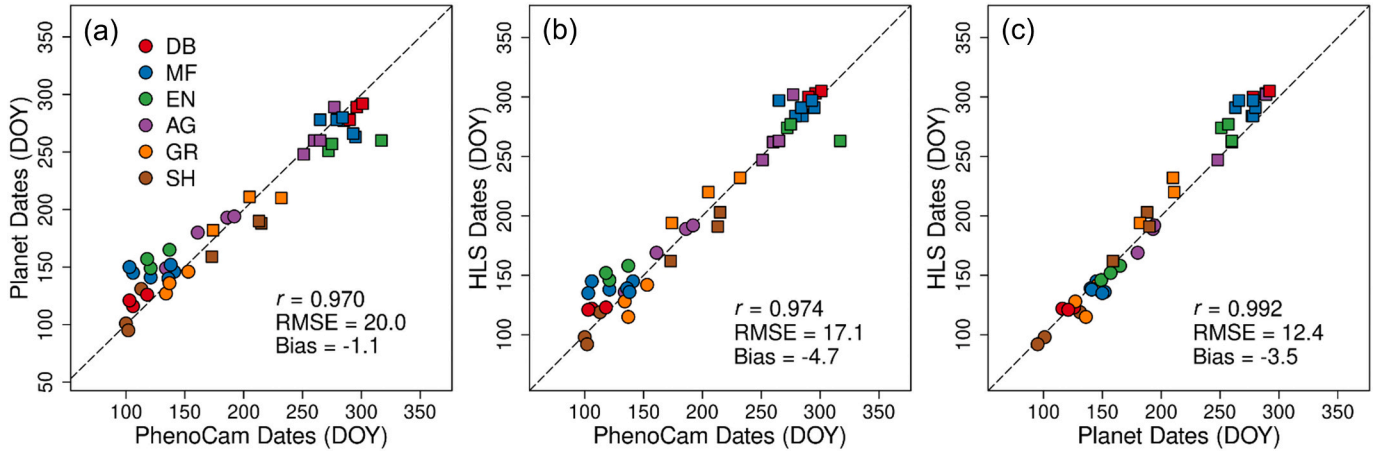

Fig. 12. Comparison of phenometrics for (a) PhenoCam versus PlanetScope (b) PhenoCam versus HLS, and (c) PlanetScope versus HLS. The values plotted compare the day of year (DOY) corresponding to 50% of EVI2 (for PlanetScope and HLS) and G_{CC} (for PhenoCam) amplitude during the greenup (circles) and greendown (squares) periods across 3 years from 2017 to 2019. Bias is the systematic difference between PhenoCam, PlanetScope, and HLS (PhenoCam – PlanetScope, PhenoCam – HLS, and PlanetScope – HLS, for panels (a), (b), and (c), respectively).

variation in phenology that is not retrieved in 30 m HLS imagery. However, for use cases focused on landscape to regional-scale dynamics in phenology (e.g., focused on integrated impacts of climate change), our results demonstrate that HLS imagery provides a high-quality basis for monitoring phenology and no added benefit is gained from the higher temporal and spatial resolution provided by PlanetScope.

Correlation among time series of EVI2 from HLS and PlanetScope and G_{CC} from PhenoCams was uniformly high across all six study sites (Figs. 2, 3, 4, and 5). This is notable because each of these data sources differs from each other in significant ways. PlanetScope imagery is acquired at daily temporal frequency and fine spatial resolution, but uses sensor technology with relatively low radiometric quality (Dash and Ogutu, 2016; Houborg and McCabe, 2018; Wang et al., 2020). HLS, on the other hand, provides imagery with excellent radiometric quality but moderate spatial resolution and lower (typically sub-weekly) frequency. PhenoCam imagery provides canopy-scale measurements at sub-daily frequency, but imagery is acquired using low-cost digital cameras mounted at oblique view angles to the canopy, which impacts the

relationship between G_{CC} and vegetation canopy properties (Keenan et al., 2014; Seyednasrollah et al., 2020a; Sonnentag et al., 2012). Given these differences, the overall strong agreement across each of these independent sources of imagery suggests that each source of imagery captures the same fundamental modes of vegetation phenology across a range of vegetation and climate types.

Across multiple growing seasons, phenometrics from PlanetScope, HLS, and PhenoCams show high agreement (Figs. 9, 10, and 12). In this context, PhenoCams are widely used as a source of high-quality ground-based observations of phenology (Hufkens et al., 2012; Liu et al., 2017; Seyednasrollah et al., 2019; Zhang et al., 2018a). The strong overall agreement between phenometrics from PhenoCams and both HLS and PlanetScope imagery supports the conclusion that both HLS and PlanetScope provide a reliable basis for monitoring land surface phenology. We found no evidence to suggest that the lower radiometric quality of PlanetScope negatively impacts the quality of phenometrics estimated from time series of PlanetScope imagery. This result aligns with recent studies described above that used PlanetScope data to study phenological processes (Chen et al., 2019; Cheng et al., 2020; Dixon et al., 2021; Wang et al., 2020).

At intra-annual time scale (i.e., for individual phenometrics), site-level agreement between phenometrics from HLS and PlanetScope was much lower than aggregate agreement across the growing season (Fig. 9 and Table 2). We attribute this result to two factors. First, because each site covers a small area (i.e., 9 km^2) selected to be representative of the PhenoCam ROIs at each site, within-site variability in each phenometric is low compared to the range of variation in phenology found in most landscapes at regional and larger scales (e.g., Bolton et al., 2020; Moon et al., 2019; Zhang et al., 2018b). Second, and more importantly, the higher spatial resolution of PlanetScope imagery captures fine-scale variation in LSP that is not resolved in HLS imagery (Figs. 7, 8, and 11). Because of this, site-level correlation between individual phenometrics from PlanetScope and HLS is low. This result is consistent with results from Cheng et al. (2020), who compared phenometrics derived from PlanetScope and Sentinel-2 at landscape scale for both the greenup and greendown (~128 km^2) and observed similar patterns of agreement.

Taken together, our results suggest that PlanetScope and HLS provide retrievals of LSP metrics that are accurate and show uniform patterns of agreement across a wide range of vegetation and climate types. Indeed, one conclusion that might be drawn from this work is that PlanetScope provides a new standard for LSP studies. However, four caveats are worth noting by readers considering the use of PlanetScope imagery for LSP applications:

- First, even though our results demonstrate that the 3 m spatial resolution provided by PlanetScope yields substantial information that is not resolved at the 30 m moderate spatial resolution provided by HLS, it is possible (or even likely) that some of the spatial detail retrieved from PlanetScope is not realistic. Specifically, the combined effects of geolocation uncertainty and day-to-day variability in PlanetScope overpass times (i.e., BRDF effects from solar geometry) introduce noise to phenometrics estimated from PlanetScope imagery. We do not quantify the magnitude of how these factors impact our results, and their impact is mitigated by the underlying LSP algorithm, which smooths the time series at each pixel. However, it is likely that LSP metrics from PlanetScope imagery are affected by variability in EVI2 time series arising from geolocation uncertainty and BRDF effects.
- Second, the utility of 3 m LSP information depends on the application. For some use cases (e.g., monitoring crops for pests), high-spatial resolution LSP information is clearly useful. However, many applications focused on monitoring and mapping regional- and larger-scale patterns and dynamics in phenology (e.g., measuring the climate sensitivity of entire ecosystems), do not require the spatial resolution afforded by PlanetScope imagery. In this context, the results from this work demonstrate that LSP results from HLS are strongly correlated and have near-zero bias with the average of 3 m LSP metrics extracted within HLS pixels derived from PlanetScope. Hence, unless fine spatial LSP information is required, our results indicate that PlanetScope imagery provides little benefit relative to HLS for investigations focused on large-scale changes in phenology.
- Third, for LSP applications applied over large areas, the cost associated with purchasing and processing 3 m daily PlanetScope imagery is likely to be prohibitive for many users in the science community. Therefore, the choice of which source of imagery is most suitable depends on (indeed, will often be dictated by) both the resources available and the application.
- Fourth, while our analysis includes a wide range of climate and plant functional types, the sites we consider are all located in the temperate zone, and more work is needed to extend these results to sites in the tropics and high latitude ecosystems.

A final consideration, which we do not address directly in this paper but is worth noting, is the role and utility of PlanetScope imagery for assessing moderate and coarse spatial resolution LSP data products. Specifically, challenges involved in collecting independent data sets that are both reliable and directly comparable to LSP results are widely documented, and assessment of LSP products has been a long-standing issue in the LSP community. In most cases, LSP product assessment has been conducted opportunistically, using large numbers of observations collected for individual plants or trees (e.g., using data from the USA National Phenology Network or the Pan European Phenological database) (Rodriguez-Galiano et al., 2015; Zhang et al., 2018b), and more recently using data from PhenoCams (Hufkens et al., 2012; Moon et al., 2019; Richardson et al., 2018b). However, issues related to representativeness and scale introduce substantial uncertainty to such assessments. Results from this study provide an excellent proof-of-concept that PlanetScope imagery provides a useful basis for assessing LSP algorithms and data products derived from coarse - (MODIS, VIIRS, Proba-V, and Sentinel-3) and moderate- (Landsat and Sentinel-2) spatial resolution imagery.

5. Conclusions

Land surface phenology is a powerful tool for monitoring and characterizing the nature, magnitude, and timing vegetation phenology over large areas at seasonal-to-decadal time scales. In recent years, the LSP community has rapidly moved towards higher resolution products based on moderate spatial resolution satellite imagery. However, the overall effectiveness and accuracy of such higher resolution imagery for estimating and monitoring LSP are not well-characterized.

In this study, we conducted a multiscale assessment of LSP metrics retrieved from Harmonized Landsat 8 and Sentinel-2 (HLS), PlanetScope, and PhenoCam imagery. The results show that overall agreement between phenometrics from each source of imagery is high, and thus indicate that data from both HLS and PlanetScope can be used with confidence to monitor LSP over large areas. HLS provides global imagery at moderate spatial resolution with high radiometric quality. However, phenometrics derived from HLS obscure fine-scale variation in LSP that occurs below the 30 m spatial resolution afforded by HLS. Our results demonstrate that the higher temporal and spatial resolution provided by PlanetScope imagery has substantial value and utility for LSP studies. However, questions related to cost and whether or not 3 m imagery is needed for many applications impose substantial constraints on widespread adoption of PlanetScope imagery for large-scale studies of phenology. In the short term, we conclude that PlanetScope provides a useful and effective basis for assessing the quality of LSP algorithms and data products at moderate and coarse spatial resolution. In the longer term, as more sources of high spatial and temporal resolution imagery become available and the LSP community develops the next generation of LSP products, it will be important to develop better understandings of where, how, and for which applications different sources of imagery are

most effective and appropriate.

Author contributions

M.M. and M.A.F designed the analysis and led the drafting of the manuscript. MM. performed the analysis. A.D.R. contributed analysis ideas and participated in drafting the manuscript.

Declaration of competing interest

The authors declare that they have no known competing financial interests or personal relationships that could have appeared to influence the work reported in this paper.

Acknowledgments

This work was supported by NASA grant #80NSSC18K0334 and by NSF award #1702627. We gratefully acknowledge the support and excellent work of the HLS team at NASA GSFC who provide the HLS data product, and without whose efforts, this work would not be possible. For use of the PhenoCam data, we thank our many collaborators, including site PIs and technicians, for their efforts in support of PhenoCam. The development of PhenoCam has been funded by the Northeastern States Research Cooperative, NSF's Macrosystems Biology Program (awards EF-1065029 and EF-1702697), and DOE's Regional and Global Climate Modeling Program (award DE-SC0016011). Additional funding, through the National Science Foundation's LTER program, has supported research at Harvard Forest (DEB-1237491). We also gratefully acknowledge NASA's Commercial Smallsat Data Acquisition (CSDA) Program, which provided access to the PlanetScope imagery used in this study.

Appendix A. Supplementary data

Supplementary data to this article can be found online at https://doi.org/10.1016/j.rse.2021.112716.

References

Berra, E.F., Gaulton, R., 2021. Remote sensing of temperate and boreal forest phenology: a review of progress, challenges and opportunities in the intercomparison of in-situ and satellite phenological metrics. For. Ecol. Manag. 480, 118663. https://doi.org/10.1016/j.foreco.2020.118663.

Bolton, D.K., Gray, J.M., Melaas, E.K., Moon, M., Eklundh, L., Friedl, M.A., 2020. Continental-scale land surface phenology from harmonized Landsat 8 and Sentinel-2 imagery. Remote Sens. Environ. 240, 111685. https://doi.org/10.1016/j.rse.2020.111685.

Breunig, F.M., Galvão, L.S., Dalagnol, R., Dauve, C.E., Parraga, A., Santi, A.L., Della Flora, D.P., Chen, S., 2020. Delineation of management zones in agricultural fields using cover–crop biomass estimates from PlanetScope data. Int. J. Appl. Earth Obs. Geoinf. 85, 102004. https://doi.org/10.1016/j.jag.2019.102004.

Cai, Y., Guan, K., Peng, J., Wang, S., Seifert, C., Wardlow, B., Li, Z., 2018. A high-performance and in-season classification system of field-level crop types using time-series Landsat data and a machine learning approach. Remote Sens. Environ. 210, 35–47. https://doi.org/10.1016/j.rse.2018.02.045.

Chaves, M., Picoli, C.A., M., D., Sanches, I., 2020. Recent applications of Landsat 8/OLI and Sentinel-2/MSI for land use and land cover mapping: a systematic review. Remote Sens. 12, 3062. https://doi.org/10.3390/rs12183062.

Chen, B., Jin, Y., Brown, P., 2019. An enhanced bloom index for quantifying floral phenology using multi-scale remote sensing observations. ISPRS J. Photogramm. Remote Sens. 156, 108–120. https://doi.org/10.1016/j.isprsjprs.2019.08.006.

Cheng, Y., Vrieling, A., Fava, F., Meroni, M., Marshall, M., Gachoki, S., 2020. Phenology of short vegetation cycles in a Kenyan rangeland from PlanetScope and Sentinel-2. Remote Sens. Environ. 248, 112004. https://doi.org/10.1016/j.rse.2020.112004.

Claverie, M., Ju, J., Masek, J.G., Dungan, J.L., Vermote, E.F., Roger, J.-C., Skakun, S.V., Justice, C., 2018. The harmonized Landsat and Sentinel-2 surface reflectance data set. Remote Sens. Environ. 219, 145–161. https://doi.org/10.1016/j.rse.2018.09.002.

Csillik, O., Asner, G.P., 2020. Near-real time aboveground carbon emissions in Peru. PLoS One 15, e0241418. https://doi.org/10.1371/journal.pone.0241418.

Dash, J., Ogutu, B.O., 2016. Recent advances in space-borne optical remote sensing systems for monitoring global terrestrial ecosystems. In: Progress in Physical Geography: Earth and Environment, 40, pp. 322–351. https://doi.org/10.1177/0309133316639403.

Diao, C., 2020. Remote sensing phenological monitoring framework to characterize corn and soybean physiological growing stages. Remote Sens. Environ. 248, 111960. https://doi.org/10.1016/j.rse.2020.111960.

Dixon, D.J., Callow, J.N., Duncan, J.M.A., Setterfield, S.A., Pauli, N., 2021. Satellite prediction of forest flowering phenology. Remote Sens. Environ. 255, 112197. https://doi.org/10.1016/j.rse.2020.112197.

Elmore, A.J., Guinn, S.M., Minsley, B.J., Richardson, A.D., 2012. Landscape controls on the timing of spring, autumn, and growing season length in mid-Atlantic forests. Glob. Chang. Biol. 18, 656–674. https://doi.org/10.1111/j.1365-2486.2011.02521.x.

Fisher, J.I., Mustard, J.F., 2007. Cross-scalar satellite phenology from ground, Landsat, and MODIS data. Remote Sens. Environ. 109, 261–273. https://doi.org/10.1016/j.rse.2007.01.004.

Friedl, M.A., 2020. MuSLI multi-source land surface phenology yearly North America 30 m V001. In: Distributed by NASA EOSDIS Land Processes DAAC. https://doi.org/10.5067/Community/MuSLI/MSLSP30NA.001.

Friedl, M.A., Gray, J.M., Melaas, E.K., Richardson, A.D., Hufkens, K., Keenan, T.F., Bailey, Amey, O'Keefe, J., 2014. A tale of two springs: using recent climate anomalies to characterize the sensitivity of temperate forest phenology to climate change. Environ. Res. Lett. 9, 054006 https://doi.org/10.1088/1748-9326/9/5/054006.

Ganguly, S., Friedl, M.A., Tan, B., Zhang, X., Verma, M., 2010. Land surface phenology from MODIS: characterization of the collection 5 global land cover dynamics product. Remote Sens. Environ. 114, 1805–1816. https://doi.org/10.1016/j.rse.2010.04.005.

Houborg, R., McCabe, M.F., 2018. A cubesat enabled spatio-temporal enhancement method (CESTEM) utilizing planet, Landsat and MODIS data. Remote Sens. Environ. 209, 211–226. https://doi.org/10.1016/j.rse.2018.02.067.

Hufkens, K., Friedl, M., Sonnentag, O., Braswell, B.H., Milliman, T., Richardson, A.D., 2012. Linking near-surface and satellite remote sensing measurements of deciduous broadleaf forest phenology. In: Remote Sensing of Environment, Remote Sensing of Urban Environments, 117, pp. 307–321. https://doi.org/10.1016/j.rse.2011.10.006.

Jiang, Z., Huete, A.R., Didan, K., Miura, T., 2008. Development of a two-band enhanced vegetation index without a blue band. Remote Sens. Environ. 112, 3833–3845. https://doi.org/10.1016/j.rse.2008.06.006.

John, A., Ong, J., Theobald, E.J., Olden, J.D., Tan, A., HilleRisLambers, J., 2020. Detecting montane flowering phenology with CubeSat imagery. Remote Sens. 12, 2894. https://doi.org/10.3390/rs12182894.

Jonsson, P., Eklundh, L., 2002. Seasonality extraction by function fitting to time-series of satellite sensor data. IEEE Trans. Geosci. Remote Sens. 40, 1824–1832. https://doi.org/10.1109/TGRS.2002.802519.

Jönsson, A.M., Eklundh, L., Hellström, M., Bärring, L., Jönsson, P., 2010. Annual changes in MODIS vegetation indices of Swedish coniferous forests in relation to snow dynamics and tree phenology. Remote Sens. Environ. 114, 2719–2730. https://doi.org/10.1016/j.rse.2010.06.005.

Justice, C.O., Townshend, J.R.G., Holben, B.N., Tucker, C.J., 1985. Analysis of the phenology of global vegetation using meteorological satellite data. Int. J. Remote Sens. 6, 1271–1318. https://doi.org/10.1080/01431168508948281.

Keenan, T.F., Darby, B., Felts, E., Sonnentag, O., Friedl, M.A., Hufkens, K., O'Keefe, J., Klosterman, S., Munger, J.W., Toomey, M., Richardson, A.D., 2014. Tracking forest phenology and seasonal physiology using digital repeat photography: a critical assessment. Ecol. Appl. 24, 1478–1489. https://doi.org/10.1890/13-0652.1.

Kimm, H., Guan, K., Jiang, C., Peng, B., Gentry, L.F., Wilkin, S.C., Wang, S., Cai, Y., Bernacchi, C.J., Peng, J., Luo, Y., 2020. Deriving high-spatiotemporal-resolution leaf area index for agroecosystems in the U.S. Corn Belt using Planet Labs CubeSat and STAIR fusion data. Remote Sens. Environ. 239, 111615. https://doi.org/10.1016/j.rse.2019.111615.

Klosterman, S.T., Hufkens, K., Gray, J.M., Melaas, E., Sonnentag, O., Lavine, I., Mitchell, L., Norman, R., Friedl, M.A., Richardson, A.D., 2014. Evaluating remote sensing of deciduous forest phenology at multiple spatial scales using PhenoCam imagery. Biogeosciences 11, 4305–4320. https://doi.org/10.5194/bg-11-4305-2014.

Liu, Y., Hill, M.J., Zhang, X., Wang, Z., Richardson, A.D., Hufkens, K., Filippa, G., Baldocchi, D.D., Ma, S., Verfaillie, J., Schaaf, C.B., 2017. Using data from Landsat, MODIS, VIIRS and PhenoCams to monitor the phenology of California oak/grass savanna and open grassland across spatial scales. Agric. For. Meteorol. 237–238, 311–325. https://doi.org/10.1016/j.agrformet.2017.02.026.

Liu, Q., Piao, S., Janssens, I.A., Fu, Y., Peng, S., Lian, X., Ciais, P., Myneni, R.B., Peñuelas, J., Wang, T., 2018. Extension of the growing season increases vegetation exposure to frost. Nat. Commun. 9, 426. https://doi.org/10.1038/s41467-017-02690-y.

Loranty, M.M., Davydov, S.P., Kropp, H., Alexander, H.D., Mack, M.C., Natali, S.M., Zimov, N.S., 2018. Vegetation indices do not capture forest cover variation in upland Siberian larch forests. Remote Sens. 10, 1686. https://doi.org/10.3390/rs10111686.

Matheron, G., 1963. Principles of geostatistics. Econ. Geol. 58, 1246–1266. https://doi.org/10.2113/gsecongeo.58.8.1246.

Melaas, E.K., Friedl, M.A., Zhu, Z., 2013. Detecting interannual variation in deciduous broadleaf forest phenology using Landsat TM/ETM+ data. Remote Sens. Environ. 132, 176–185. https://doi.org/10.1016/j.rse.2013.01.011.

Melaas, E.K., Sulla-Menashe, D., Gray, J.M., Black, T.A., Morin, T.H., Richardson, A.D., Friedl, M.A., 2016. Multisite analysis of land surface phenology in North American temperate and boreal deciduous forests from Landsat. Remote Sens. Environ. 186, 452–464. https://doi.org/10.1016/j.rse.2016.09.014.

Milliman, T., Seyednasrollah, B., Young, A.M., Hufkens, K., Friedl, M.A., Frolking, S., Richardson, A.D., Abraha, M., Allen, D.W., Apple, M., Arain, M.A., Baker, J., Baker, J.M., Bernacchi, C.J., Bhattacharjee, J., Blanken, P., Bosch, D.D.,

Boughton, R., Boughton, E.H., Brown, R.F., Browning, D.M., Brunsell, N., Burns, S.P., Cavagna, M., Chu, H., Clark, P.E., Conrad, B.J., Cremonese, E., Debinski, D., Desai, A.R., Diaz-Delgado, R., Duchesne, L., Dunn, A.L., Eissenstat, D.M., El-Madany, T., Ellum, D.S.S., Ernest, S.M., Esposito, A., Fenstermaker, L., Flanagan, L. B., Forsythe, B., Gallagher, J., Gianelle, D., Griffis, T., Groffman, P., Gu, L., Guillemot, J., Halpin, M., Hanson, P.J., Hemming, D., Hove, A.A., Humphreys, E.R., Jaimes-Hernandez, A., Jaradat, A.A., Johnson, J., Keel, E., Kelly, V.R., Kirchner, J. W., Kirchner, P.B., Knapp, M., Krassovski, M., Langvall, O., Lanthier, G., Maire, G.L., Magliulo, E., Martin, T.A., Mcneil, B., Meyer, G.A., Migliavacca, M., Mohanty, B.P., Moore, C.E., Mudd, R., Munger, J.W., Murrell, Z.E., Nesic, Z., Neufeld, H.S., Oechel, W., Oishi, A.C., Oswald, W.W., Perkins, T.D., Reba, M.L., Rundquist, B., Runkle, B.R., Russell, E.S., Sadler, E.J., Saha, A., Saliendra, N.Z., Schmalbeck, L., Schwartz, M.D., Scott, R.L., Smith, E.M., Sonnentag, O., Stoy, P., Strachan, S., Suvocarev, K., Thom, J.E., Thomas, R.Q., Van Den Berg, A.K., Vargas, R., Vogel, C.S., Walker, J.J., Webb, N., Wetzel, P., Weyers, S., Whipple, A.V., Whitham, T.G., Wohlfahrt, G., Wood, J.D., Yang, J., Yang, X., Yenni, G., Zhang, Y., Zhang, Q., Zona, D., Baldocchi, D., Verfaillie, J., 2019. PhenoCam Dataset v2.0: Digital Camera Imagery from the PhenoCam Network, 2000–2018. ORNL DAAC. https://doi.org/10.3334/ORNLDAAC/1689.

Moon, M., Zhang, X., Henebry, G.M., Liu, L., Gray, J.M., Melaas, E.K., Friedl, M.A., 2019. Long-term continuity in land surface phenology measurements: a comparative assessment of the MODIS land cover dynamics and VIIRS land surface phenology products. Remote Sens. Environ. 226, 74–92. https://doi.org/10.1016/j.rse.2019.03.034.

Moon, M., Li, D., Liao, W., Rigden, A.J., Friedl, M.A., 2020. Modification of surface energy balance during springtime: the relative importance of biophysical and meteorological changes. Agric. For. Meteorol. 284, 107905. https://doi.org/10.1016/j.agrformet.2020.107905.

Moon, M., Seyednasrollah, B., Richardson, A.D., Friedl, M.A., 2021. Using time series of MODIS land surface phenology to model temperature and photoperiod controls on spring greenup in North American deciduous forests. Remote Sens. Environ. 260, 112466. https://doi.org/10.1016/j.rse.2021.112466.

Morisette, J.T., Richardson, A.D., Knapp, A.K., Fisher, J.I., Graham, E.A., Abatzoglou, J., Wilson, B.E., Breshears, D.D., Henebry, G.M., Hanes, J.M., Liang, L., 2009. Tracking the rhythm of the seasons in the face of global change: phenological research in the 21st century. Front. Ecol. Environ. 7, 253–260. https://doi.org/10.1890/070217.

Myers, E., Kerekes, J., Daughtry, C., Russ, A., 2019. Assessing the impact of satellite revisit rate on estimation of corn phenological transition timing through shape model fitting. Remote Sens. 11, 2558. https://doi.org/10.3390/rs11212558.

Nguyen, L.H., Joshi, D.R., Clay, D.E., Henebry, G.M., 2020. Characterizing land cover/land use from multiple years of Landsat and MODIS time series: a novel approach using land surface phenology modeling and random forest classifier. In: Remote Sensing of Environment, Time Series Analysis With High Spatial Resolution Imagery, 238, p. 111017. https://doi.org/10.1016/j.rse.2018.12.016.

Park, T., Ganguly, S., Tømmervik, H., Euskirchen, E.S., Høgda, K.-A., Karlsen, S.R., Brovkin, V., Nemani, R.R., Myneni, R.B., 2016. Changes in growing season duration and productivity of northern vegetation inferred from long-term remote sensing data. Environ. Res. Lett. 11, 084001 https://doi.org/10.1088/1748-9326/11/8/084001.

Piao, S., Liu, Q., Chen, A., Janssens, I.A., Fu, Y., Dai, J., Liu, L., Lian, X., Shen, M., Zhu, X., 2019. Plant phenology and global climate change: current progresses and challenges. Glob. Chang. Biol. https://doi.org/10.1111/gcb.14619.

Pickering, J., Tyukavina, A., Khan, A., Potapov, P., Adusei, B., Hansen, M.C., Lima, A., 2021. Using multi-resolution satellite data to quantify land dynamics: applications of PlanetScope imagery for cropland and tree-cover loss area estimation. Remote Sens. 13, 2191. https://doi.org/10.3390/rs13112191.

Planet, 2021. Satellite Imagery and Archive [WWW Document]. Planet. URL. https://planet.com/products/planet-imagery/ (accessed 5.17.21).

Qayyum, N., Ghuffar, S., Ahmad, H.M., Yousaf, A., Shahid, I., 2020. Glacial lakes mapping using multi satellite PlanetScope imagery and deep learning. ISPRS Int. J. Geo Inf. 9, 560. https://doi.org/10.3390/ijgi9100560.

Reed, B.C., Brown, J.F., VanderZee, D., Loveland, T.R., Merchant, J.W., Ohlen, D.O., 1994. Measuring phenological variability from satellite imagery. J. Veg. Sci. 5, 703–714. https://doi.org/10.2307/3235884.

Richardson, A.D., Keenan, T.F., Migliavacca, M., Ryu, Y., Sonnentag, O., Toomey, M., 2013. Climate change, phenology, and phenological control of vegetation feedbacks to the climate system. Agric. For. Meteorol. 169, 156–173. https://doi.org/10.1016/j.agrformet.2012.09.012.

Richardson, A.D., Hufkens, K., Milliman, T., Aubrecht, D.M., Chen, M., Gray, J.M., Johnston, M.R., Keenan, T.F., Klosterman, S.T., Kosmala, M., Melaas, E.K., Friedl, M. A., Frolking, S., 2018a. Tracking vegetation phenology across diverse North American biomes using PhenoCam imagery. Sci. Data 5, 180028. https://doi.org/10.1038/sdata.2018.28.

Richardson, A.D., Hufkens, K., Milliman, T., Frolking, S., 2018b. Intercomparison of phenological transition dates derived from the PhenoCam Dataset V1.0 and MODIS satellite remote sensing. Sci. Rep. 8, 5679. https://doi.org/10.1038/s41598-018-23804-6.

Rodriguez-Galiano, V.F., Dash, J., Atkinson, P.M., 2015. Intercomparison of satellite sensor land surface phenology and ground phenology in Europe. Geophys. Res. Lett. 42, 2253–2260. https://doi.org/10.1002/2015GL063586.

Sadeh, Y., Zhu, X., Dunkerley, D., Walker, J.P., Zhang, Y., Rozenstein, O., Manivasagam, V.S., Chenu, K., 2021. Fusion of Sentinel-2 and PlanetScope time-series data into daily 3 m surface reflectance and wheat LAI monitoring. Int. J. Appl. Earth Obs. Geoinf. 96, 102260. https://doi.org/10.1016/j.jag.2020.102260.

Seyednasrollah, B., Young, A.M., Hufkens, K., Milliman, T., Friedl, M.A., Frolking, S., Richardson, A.D., 2019. Tracking vegetation phenology across diverse biomes using Version 2.0 of the PhenoCam Dataset. Sci. Data 6, 222. https://doi.org/10.1038/s41597-019-0229-9.

Seyednasrollah, B., Bowling, D.R., Cheng, R., Logan, B.A., Magney, T.S., Frankenberg, C., Yang, J.C., Young, A.M., Hufkens, K., Arain, M.A., Black, T.A., Blanken, P.D., Bracho, R., Jassal, R., Hollinger, D.Y., Law, B.E., Nesic, Z., Richardson, A.D., 2020a. Seasonal variation in the canopy color of temperate evergreen conifer forests. New Phytol. https://doi.org/10.1111/nph.17046 n/a.

Seyednasrollah, B., Young, A.M., Li, X., Milliman, T., Ault, T., Frolking, S., Friedl, M., Richardson, A.D., 2020b. Sensitivity of deciduous forest phenology to environmental drivers: implications for climate change impacts across North America. Geophys. Res. Lett. 47 https://doi.org/10.1029/2019GL086788.

Seyednasrollah, B., Bowling, D.R., Cheng, R., Logan, B.A., Magney, T.S., Frankenberg, C., Yang, J.C., Young, A.M., Hufkens, K., Arain, M.A., Black, T.A., Blanken, P.D., Bracho, R., Jassal, R., Hollinger, D.Y., Law, B.E., Nesic, Z., Richardson, A.D., 2021. Seasonal variation in the canopy color of temperate evergreen conifer forests. New Phytol. 229, 2586–2600. https://doi.org/10.1111/nph.17046.

Sonnentag, O., Hufkens, K., Teshera-Sterne, C., Young, A.M., Friedl, M., Braswell, B.H., Milliman, T., O'Keefe, J., Richardson, A.D., 2012. Digital repeat photography for phenological research in forest ecosystems. Agric. For. Meteorol. 152, 159–177. https://doi.org/10.1016/j.agrformet.2011.09.009.

Sulla-Menashe, D., Gray, J.M., Abercrombie, S.P., Friedl, M.A., 2019. Hierarchical mapping of annual global land cover 2001 to present: the MODIS collection 6 land cover product. Remote Sens. Environ. 222, 183–194. https://doi.org/10.1016/j.rse.2018.12.013.

USDA, 2020. USDA National Agricultural Statistics Service Cropland Data Layer [WWW Document]. Crop-specific Data Layer. URL. https://nassgeodata.gmu.edu/CropScape/ (accessed 5.17.21).

USGS, Rigge, M., 2019. National Land Cover Database (NLCD) 2016 Shrubland Fractional Components for the Western U.S. (ver. 3.0, July 2020): U.S. Geological Survey Data Release. https://doi.org/10.5066/P9MJVQSQ.

Wang, J., Yang, D., Detto, M., Nelson, B.W., Chen, M., Guan, K., Wu, S., Yan, Z., Wu, J., 2020. Multi-scale integration of satellite remote sensing improves characterization of dry-season green-up in an Amazon tropical evergreen forest. Remote Sens. Environ. 246, 111865. https://doi.org/10.1016/j.rse.2020.111865.

Wicaksono, P., Lazuardi, W., 2018. Assessment of PlanetScope images for benthic habitat and seagrass species mapping in a complex optically shallow water environment. Int. J. Remote Sens. 39, 5739–5765. https://doi.org/10.1080/01431161.2018.1506951.

Wu, S., Wang, J., Yan, Z., Song, G., Chen, Y., Ma, Q., Deng, M., Wu, Y., Zhao, Y., Guo, Z., Yuan, Z., Dai, G., Xu, X., Yang, X., Su, Y., Liu, L., Wu, J., 2021. Monitoring tree-crown scale autumn leaf phenology in a temperate forest with an integration of PlanetScope and drone remote sensing observations. ISPRS J. Photogramm. Remote Sens. 171, 36–48. https://doi.org/10.1016/j.isprsjprs.2020.10.017.

Young, A.M., Friedl, M.A., Seyednasrollah, B., Beamesderfer, E., Carrillo, C.M., Li, X., Moon, M., Arain, M.A., Baldocchi, D.D., Blanken, P.D., Bohrer, G., 2021. Seasonality in aerodynamic resistance across a range of North American ecosystems. Agric. For. Meteorol. 310, 108613.

Zeng, L., Wardlow, B.D., Xiang, D., Hu, S., Li, D., 2020. A review of vegetation phenological metrics extraction using time-series, multispectral satellite data. Remote Sens. Environ. 237, 111511. https://doi.org/10.1016/j.rse.2019.111511.

Zhang, X., Friedl, M.A., Schaaf, C.B., Strahler, A.H., Hodges, J.C.F., Gao, F., Reed, B.C., Huete, A., 2003. Monitoring vegetation phenology using MODIS. Remote Sens. Environ. 84, 471–475. https://doi.org/10.1016/S0034-4257(02)00135-9.

Zhang, X., Jayavelu, S., Liu, L., Friedl, M.A., Henebry, G.M., Liu, Y., Schaaf, C.B., Richardson, A.D., Gray, J., 2018a. Evaluation of land surface phenology from VIIRS data using time series of PhenoCam imagery. Agric. For. Meteorol. 256–257, 137–149. https://doi.org/10.1016/j.agrformet.2018.03.003.

Zhang, X., Liu, L., Liu, Y., Jayavelu, S., Wang, J., Moon, M., Henebry, G.M., Friedl, M.A., Schaaf, C.B., 2018b. Generation and evaluation of the VIIRS land surface phenology product. Remote Sens. Environ. 216, 212–229. https://doi.org/10.1016/j.rse.2018.06.047.

Zhu, Z., Woodcock, C.E., 2014. Continuous change detection and classification of land cover using all available Landsat data. Remote Sens. Environ. 144, 152–171. https://doi.org/10.1016/j.rse.2014.01.011.